Uncovering Shared and Tissue-Specific Molecular Adaptations to Intermittent Fasting in Liver, Brain, and Muscle

Yibo Fan[1,2,$], Senuri De Silva[3,4,$], Nishat I. Tabassum[1,2], Xiangyuan Peng[1,2], Vernise Lim[1,2], Xiangru Cheng[1,2], Keshava K. Datta[5], Rohan Lowe[5], Terrance G. Johns[6], Mark P. Mattson[7], Suresh Mathivanan[1], Christopher G. Sobey[1,8,9], Eitan Okun[10], Yong U. Liu[11], Guobing Chen[12], Mitchell K. P. Lai[13], Dong-Gyu Jo[14], Jayantha Gunaratne[3,4,*], Thiruma V. Arumugam[1,2,14,*]

[1] Department of Microbiology, Anatomy, Physiology and Pharmacology, School of Agriculture, Biomedicine and Environment, La Trobe University, Melbourne, Australia.
[2] La Trobe Institute for Molecular Science, La Trobe University, Melbourne, Australia.
[3] Translational Biomedical Proteomics Laboratory, Institute of Molecular and Cell Biology, Agency for Science, Technology and Research, Singapore, Singapore.
[4] Department of Anatomy, Yong Loo Lin School of Medicine, National University of Singapore, Singapore, Singapore.
[5] La Trobe University-Proteomics and Metabolomics Platform (LTU-PMP), La Trobe Institute for Molecular Science, La Trobe University, Melbourne, Australia.
[6] Epigenes Australia Pty Ltd., Melbourne, Victoria, Australia.
[7] Department of Neuroscience, Johns Hopkins University School of Medicine, Baltimore, MD, USA.
[8] Centre for Cardiovascular Biology and Disease Research, La Trobe Institute for Molecular Sciences, La Trobe University, Bundoora, Victoria, 3086, Australia.
[9] Baker Heart and Diabetes Institute, Melbourne, Victoria, 3004, Australia
[10] The Paul Feder laboratory for Alzheimer's disease research at the Mina and Everard Goodman Faculty of Life Sciences, and the Leslie and Susan Gonda Multidisciplinary Brain Research Center, Bar Ilan University, Ramat Gan, Israel.
[11] Laboratory for Neuroimmunology in Health and Diseases, Center for Medical Research on Innovation and Translation, The Second Affiliated Hospital, School of Medicine, South China University of Technology, Guangzhou, China.
[12] Department of Microbiology and Immunology, School of Medicine; Institute of Geriatric Immunology, School of Medicine, Jinan University, Guangzhou, China.
[13] Department of Pharmacology, Yong Loo Lin School of Medicine, National University of Singapore, Singapore, Singapore.
[14] School of Pharmacy, Sungkyunkwan University, Suwon, Republic of Korea.

[$] These authors (YF and SDS) contributed equally.

[#] **Corresponding authors:** Thiruma V. Arumugam**,** Centre for Cardiovascular Biology and Disease Research, La Trobe Institute for Molecular Science and Department of Microbiology, Anatomy, Physiology and Pharmacology, School of Agriculture, Biomedicine and Environment, La Trobe University, Bundoora, VIC, Australia. **E-mail:** g.arumugam@latrobe.edu.au; garriearumugam@gmail.com; or Jayantha Gunaratne, Translational Biomedical Proteomics Laboratory, Institute of Molecular and Cell Biology, Agency for Science, Technology and Research, Singapore, Singapore. **E-mail:** jayanthag@imcb.a-star.edu.sg

Keywords: Intermittent Fasting, Proteomics, Transcriptomics, Metabolic reprogramming, Serpin A1c, Bioinformatics

Abstract

Intermittent fasting (IF) has emerged as a powerful dietary intervention with profound metabolic benefits, yet the tissue-specific molecular mechanisms underlying these effects remain poorly understood. In this study, we employed comprehensive proteomics and transcriptomics analysis to investigate the systemic and organ-specific adaptations to IF in male C57BL/6 mice. Following a 16-hour daily fasting regimen (IF16) over four months, IF reduced blood glucose, HbA1c, and cholesterol levels while increasing ketone bodies, indicative of enhanced metabolic flexibility. Proteomic profiling of the liver, skeletal muscle, and cerebral cortex revealed tissue-specific responses, with the liver exhibiting the most pronounced changes, including upregulation of pathways involved in fatty acid oxidation, ketogenesis, and glycan degradation, and downregulation of steroid hormone and cholesterol metabolism. In muscle, IF enhanced pyruvate metabolism, fatty acid biosynthesis, and AMPK signaling, while suppressing oxidative phosphorylation and thermogenesis. The cerebral cortex displayed unique adaptations, with upregulation of autophagy, PPAR signaling, and metabolic pathways, and downregulation of TGF-beta and p53 signaling, suggesting a shift toward energy conservation and stress resilience. Notably, Serpin A1c emerged as the only protein commonly upregulated across all three tissues, highlighting its potential role in systemic adaptation to IF. Integrative transcriptomic and proteomic analyses revealed partial concordance between mRNA and protein expression, underscoring the complexity of post-transcriptional regulation. Shared biological signaling processes were identified across tissues, suggesting unifying mechanisms linking metabolic changes to cellular communication. Our findings reveal both conserved and tissue-specific responses by which IF may optimize energy utilization, enhance metabolic flexibility, and promote cellular resilience.

Introduction

In recent decades, the global aging population has increased dramatically, resulting in a corresponding rise in age-related diseases. Age-related decline in the functional capacity of vital organs, including the brain, liver, and skeletal muscle, is well documented and attributed to several interrelated mechanisms including cellular senescence, oxidative stress, mitochondrial dysfunction, and diminished regenerative capacity (López-Otín et al., 2023).

Intermittent fasting (IF) has emerged as a promising intervention that can improve health and counteract disease processes in both rodents and humans (Mattson, 2022). Evidence suggests that IF confers protection against a range of age-associated diseases by bolstering cellular stress resistance, enhancing autophagy, and promoting cell growth and plasticity (Mattson, 2025); Longo et al., 2014). During IF, liver glycogen stores are depleted, leading to low circulating glucose levels, while adipocytes mobilize fatty acids (Anton et al., 2018). These fatty acids are subsequently converted in the liver into the ketone bodies β-hydroxybutyrate (BHB) and acetoacetate (AcAc), which enter the bloodstream and are utilized as alternative energy substrates by neurons and other cell types. This metabolic shift, characterized by the transition from carbohydrate and glucose utilization to the reliance on fatty acids and ketones, is referred to as the metabolic switch (Mattson et al., 2018).

Intermittent metabolic switching enhances physiological functions across multiple organ systems by regulating the expression of specific genes and proteins (Mattson, 2025). IF-induced metabolic switching has been shown to upregulate genes involved in organ remodeling, influencing key metabolic pathways such as AMPK signaling, insulin signaling, and cellular signaling cascades involving protein chaperones and trophic factors (Mattson et al., 2018). These IF-mediated alterations in gene expression are likely influenced by changes in the epigenetic landscape, including DNA methylation and histone modifications (Asif et al., 2020). Furthermore, our recent deep proteomic and phosphoproteomic analyses of heart tissue revealed multiple adaptive responses of cardiac cells to IF (Arumugam et al., 2023). While these studies shed light on the mechanistic foundations of IF, a comprehensive and systematic analysis is needed to identify the unique and shared protein changes of cells in various organs in response to IF.

This study explores the proteomic and transcriptomic responses to IF of three distinct organ systems the liver, the brain, and skeletal muscle. By systematically analyzing expression patterns in response to IF, we identified differentially expressed proteins (DEPs) and investigated their roles in metabolic and cell signaling pathways. Through comparative analysis of these proteins across the three organs, we uncovered critical processes that may underlie the health benefits of IF. Our integrative approach revealed both common and tissue-specific protein network of common and unique proteins that link IF to systemic physiological effects. To our knowledge, this is the first study that provides a comprehensive understanding of how

IF modulates proteomes across multiple organs, offering novel insights into the molecular mechanisms driving its health-promoting effects.

Materials and methods

Experimental Design and Animal Procedures

The *in vivo* experiments described here received ethical approval from the Animal Care and Use Committee at La Trobe University (Approval ID: AEC21047) and adhered to the standards set by the Australian Code for the Care and Use of Animals for Scientific Purposes (8th edition) as well as the NIH Guide for the Care and Use of Laboratory Animals. Measures were taken to limit animal suffering and optimize the number of animals involved. The study complied with the ARRIVE guidelines throughout all stages of the research. Male C57BL/6 mice, aged 4 weeks, were sourced from the Animal Resources Centre in Australia and maintained at La Trobe University's animal housing facility. They were kept under a 12-hour light/12-hour dark schedule (lights on from 07:00 to 19:00) and fed a standard diet containing 20% crude protein, 5% crude fat, 6% crude fiber, 0.5% added salt, 0.8% calcium, and 0.45% phosphorus (Ridley, Victoria, Australia), with unrestricted access to water. At 6 weeks of age, the mice were randomly divided into two dietary groups: one undergoing intermittent fasting for 16 hours daily from 16:00 to 8:00 (IF) and a control group with unlimited food access (ad libitum, AL). Body weight was routinely measured, and blood levels of glucose and ketones were evaluated using the FreeStyle Optium Neo device along with corresponding FreeStyle Optium test strips for glucose and ketones (Abbott Laboratories, Illinois, USA), measured after a 6-hour fast. In addition, cholesterol levels were determined using the Roche Cobas b 101 Lipid system (Cat. No. ROC06380115190, Roche Diagnostics, Basel, Switzerland), while HbA1c concentrations were assessed with the Roche Cobas b 101 HbA1c (Cat. No. ROC08038694190) kits (Roche Diagnostics, Basel, Switzerland). Following the 4-month dietary phase euthanasia was carried out via carbon dioxide (CO2) inhalation between 07:00 and 12:00. Immediately afterwards, the mice were perfused with chilled PBS, and tissue samples were quickly frozen in liquid nitrogen before being stored at -80 °C for subsequent analysis.

Tissue Lysate Preparation

Tissue samples (30-50 mg) were lysed in 250 µl lysis buffer (6 M guanidine (Merck, Victoria, Australia), 100mM Tris (Merck, Victoria, Australia), 10 mM TCEP (Merck, Victoria, Australia), 40 mM 2-choloroacetamide (Merck, Victoria, Australia) pH 8.5, then homogenized,

sonicated and heated at 95°C for 5 min. Then samples were centrifuged at 20,000 g for 30 min at 4°C and the supernatant was collected. BCA assay (Thermo-Fisher Scientific, Waltham, MA, USA) was performed according to the kit's instructions to determine the protein concentration, then the samples were diluted and used for further analysis.

Mass Spectrometry (MS)-based proteomics analysis

MS-based proteomics analysis was carried out by the La Trobe University-Proteomics and Metabolomics Platform using their established workflows. Briefly, the single pot, solid phase, sample preparation strategy (Hughes et al., 2019) was used to clean up alkylated lysates before digestion. Proteins were captured on carboxylate-modified magnetic SpeedBeads (Cytiva 65152105050250 and 45152105050250) in a 50% ethanol environment by incubating at 24°C for 5 min with shaking (900 rpm). Using a magnetic rack for separations, the beads were isolated and the supernatant discarded. The beads were washed 3 times with 80% ethanol, discarding the supernatant each time. Proteins were digested with trypsin (1:20 enzyme:protein ratio) was added in 20 mM ammonium bicarbonate and incubated at 37C overnight on a shaker. The peptide solution was separated from the beads and collected into fresh tubes. Digested samples were acidified by addition of trifluoroacetic acid to 0.5% (v/v). The tryptic peptides were then desalted using the StageTip method (Rappsilber et al., 2007) and dried in a Speedvac.

LC-MS Analysis of Peptides

LC-MS was performed on a Thermo Ultimate 3000 RSLCnano UHPLC system and a Thermo Orbitrap Eclipse Tribrid mass spectrometer (Thermo-Fisher Scientific, Waltham, MA, USA) at the La Trobe University-Proteomics and Metabolomics Platform. Peptides were reconstituted in 0.1% (v/v) trifluoroacetic acid (TFA) and 2% (v/v) acetonitrile (ACN), and 500 ng of peptides were loaded onto a PepMap C18 5 µm 1 cm trapping cartridge (Thermo-Fisher Scientific, Waltham, MA, USA) at 12 µL/min for 6 min before switching the trap in-line with the analytical column (nanoEase M/Z Peptide BEH C18 Column, 1.7 µm, 130 Å and 75 µm ID × 25 cm; Waters). The column compartment was held at 55°C for the entire analysis. The separation of peptides was performed at 250 nL/min using a linear ACN gradient of buffer A (0.1% (v/v) formic acid, 2% (v/v) ACN) and buffer B (0.1% (v/v) formic acid, 80% (v/v) ACN), starting at 14% buffer B to 35% over 90 min, then rising to 50% buffer B over 15 min followed by 95% buffer B in 5 min. The column was then cleaned for 5 min at 95% buffer B and afterward a ramped down to 1% buffer B over 2 min and then held at 1% buffer B for a final 3 min.

Mass-spectra were collected on the Thermo Orbitrap Eclipse in Data Independent Acquisition (DIA) mode on the Orbitrap for both MS1 or "master scan" spectra and HCD DIA spectra. MS1 "master" scan parameters were: scan range of 350-1400 m/z, 120,000 resolution, max injection time 50 ms, AGC target 1e6 (250%). DIA spectra were collected with a target cycle time of 3s, resolution of 30K, isolation window of 15, and 45 windows covering precursor range of 361-1036 m/z, and scan range of 197-2000. AGC target set to 1e6 (2000%), max IT of 55 ms, HCD collision energy set to 30%. Internal mass correction was performed with the Thermo EASY-IC option.

Database Search

The mass-spectral database search was conducted using DIA-NN v181 (Demichev et al., 2020), with label-free DIA matching against the *Mus musculus* reference proteome downloaded from Uniprot (UP000000589_10090, 1 protein sequence per gene, March 2023). Spectral library was generated with deep-learning in DIA-NN from the fasta file and library precursors reannotated from the fasta database. min-max fragment size was 200 m/z to 1800 m/z), N-term methionine excision enabled, min-max peptide length was 7-30, min-max precursor m/z was 300-1800, precursor charge range 1-4, digest trypsin/P, missed cleavages set to 2. Fixed peptide modifications were carbamidomethyl of cysteine, and variable mods were acetylation of protein N-terminus and oxidation of methionine, and one variable mod per peptide was allowed. Processing parameters turned on were: "use quant", "peptidoforms", "reanalyse", "relaxed protein inference", and "smart profiling". Mass tolerances were determined from the dataset. Protein validation FDR threshold was 0.01.

Statistical and Differential Expression Analysis of Proteomics Data

Processed MS data (by the La Trobe University-Proteomics and Metabolomics Platform) were subjected to downstream statistical and bioinformatics analysis using JG lab established pipelines. For these analyses, the label-free intensities of all identified proteins were log-transformed, followed by median normalization across samples using the normalizeMedianValues function in limma R package (Ritchie et al., 2015). The datasets were filtered for 50% valid values across all samples (proteins with >50% missing values were excluded from downstream statistical analysis), with the remaining missing values imputed as described by Tyanova et al. (2016). All preprocessing steps were conducted within the publicly available FlexStat web application (De Silva et al., 2024). For differential protein expression

analysis in response to IF, the limma package employed within FlexStat web application was used. Pairwise comparisons against the AL control group were performed, with statistical significance assessed using the Benjamini-Hochberg procedure to control the false discovery rate (FDR), applying an adjusted p-value threshold of <0.05.

Heat Map Generation and Functional Enrichment Analyses

Heatmaps were generated using the normalized protein intensities in R with the pheatmap package (Raivo, 2018) with default parameters. DEPs were clustered to highlight expression patterns across experimental conditions. To infer potential biological functions associated with protein expression changes, Gene Ontology (GO) and Kyoto Encyclopedia of Genes and Genomes (KEGG) pathway enrichment analyses were performed. GO and KEGG enrichment analyses were conducted using the clusterProfiler R package (Yu et al., 2012), evaluating biological processes, cellular components, and molecular functions. GO terms and KEGG pathways with a q-value < 0.05 were considered significantly enriched among DEPs, indicating potential functional relevance.

To explore functional networks across different IF regimens, gene set enrichment analysis (GSEA) was performed using GSEA (version 4.3.3) desktop application on the proteomic dataset with curated mouse GO biological processes and pathway databases (version 2023.2) (Merico et al., 2010). The FDR was controlled at 0.05. Enrichment scores were assigned to each functional group, where positive scores approaching +1 indicated significant enrichment and negative scores approaching –1 indicated depletion (Subramanian et al., 2005). Pairwise comparisons of enrichment scores between experimental groups were evaluated using permutation testing. Based on gene set similarity (p-value < 0.01), EnrichmentMap plugin (Merico et al., 2010) (version 3.5.0), implemented in Cytoscape (version 3.10), was used to visualize overlapping gene set clusters, enabling network-based interpretation of enriched pathways.

Protein-Protein Interaction Network Analyses

Functional connectivity among significantly altered proteins was assessed using protein-protein interaction (PPI) data curated from the STRING database (Szklarczyk et al., 2023), which integrates experimental evidence, computational predictions, and text mining. IF-altered functional network for each organ was constructed to encompass interactions relevant to metabolic, regulatory, and signaling pathways. Redundant interactions were removed to

minimize network complexity, and IF-specific alterations in protein expression for each organ were incorporated to generate time-resolved functional networks. Only interactions with a confidence score >0.8 were included. Network visualization was performed using the STRING plugin (version 2.2.0) implemented in Cytoscape (Doncheva et al., 2019). Venn diagrams were generated to identify overlapping proteins, DEPs across different IF regimens and corresponding enriched GO terms using the InteractiVenn web application (Heberle et al., 2015).

Total RNA Extraction and Quality Control for Transcriptome Analysis

TRIzol RNA Isolation kit (Thermo-Fisher Scientific, Waltham, MA, USA) was used according to the kit's instructions to extract total RNA from liver, muscle and cerebral cortex samples. To assess the quality of the extracted total RNA, RNA purity was determined using Nanodrop ND-1000 (Thermo-Fisher Scientific, Waltham, MA, USA). Enriched RNA was of high quality, demonstrating an OD260/OD280 ratio of 1.9–2.0 from Nanodrop readings.

cDNA Library Preparation and RNA Sequencing

NEBNext Ultra II RNA Library Prep Kit for Illumina (New England BioLabs, MA, USA) and NEBNext® Ultra™II Directional RNA Library Prep Kit (New England BioLabs, MA, USA) were used according to the kit's instructions for Eukaryotic RNA-seq. Poly-T oligo-attached magnetic beads were used to purify the mRNA from total RNA. Then, a fragmentation buffer was added to the mRNA. First-strand cDNA was subsequently synthesized using random hexamer primer. Next, second-strand cDNA synthesis was performed using dUTP for directional library. After end repair, A-tailing, adapter ligation, size selection, USER enzyme digestion, amplification and purification, the library preparation was done. The library was checked with Qubit and real-time PCR for quantification and bioanalyzer for size distribution detection. Quantified libraries were pooled and sequenced on Illumina platforms, according to effective library concentration and data amount.

Transcriptome Data Mapping and Differential Expression Analysis

The RNA sequencing results from the Illumina NovaSeq 6000 Sequencing System were output as quality and color space fasta files. The files were mapped to the Ensembl-released mouse genome sequence and annotation (Mus musculus; GRCm39/mm39). Hisat2 version 2.0.5 (Kim et al., 2019) was used to build index of reference genome and align paired-end clean 1 reads to the reference genome. FeatureCounts version 1.5.0-p3 (Liao et al, 2014) was used for the

quantification of gene expression levels to count the read numbers mapped of each gene. Then FPKMs of each gene were calculated based on the length of the gene and reads count mapped to the same gene. DESeq2 R Package version.1.10.1 (Love et al., 2014) was used to perform differential expression analysis. Genes with p-value <0.05 found by DESeq2 were assigned as differentially expressed.

Integrative Analysis of Proteome and Transcriptome Data

To integrate the proteome and transcriptome datasets, we focused on differentially expressed genes (DEGs) and proteins (DEPs) that met a significance threshold of $p < 0.05$. Only DEGs with corresponding DEPs were included in the analysis. For comparative analysis of transcriptome and proteome changes between the IF and AL groups, the VennDiagram R package version 3.0.3 (Chen et al., 2011) was employed to identify overlapping genes between the proteome and transcriptome datasets. This allowed us to pinpoint genes that were consistently regulated at both the mRNA and protein levels.

To visualize expression patterns, heatmaps were generated using normalized protein intensities for the proteome data and raw FPKM (Fragments Per Kilobase of transcript per Million mapped reads) values for the transcriptome data. Heatmaps were constructed using the pheatmap R package (Raivo, 2018) with default parameters. DEPs and DEGs were clustered separately to highlight distinct expression profiles across the experimental conditions. To infer the potential biological functions of the overlapping genes, Kyoto Encyclopedia of Genes and Genomes (KEGG) pathway enrichment analysis was performed. This analysis was conducted using the clusterProfiler R package (Yu et al., 2012). KEGG pathways with a p-value < 0.05 were considered significantly enriched, indicating potential functional relevance of the overlapping genes in the context of the studied conditions. This integrative approach provided insights into the molecular mechanisms underlying the observed changes in gene and protein expression.

Immunohistochemistry

Following transcardiac perfusion fixation, liver tissue was dissected and cryoprotected overnight in 30% (w/v) sucrose in phosphate-buffered saline (PBS). Horizontal cryostat sections (14 μm thickness) were prepared and mounted on slides. For immunofluorescence staining, sections underwent antigen retrieval followed by incubation with a polyclonal anti-α-1 antitrypsin primary antibody (PA5-122246, 1:50 dilution). Signal detection was performed

using an Alexa Fluor 488-conjugated secondary antibody (ab150081). Images were acquired on a Zeiss LSM 780 confocal microscope and processed using ZEN 2011 Blue Edition software (Carl Zeiss AG).

Statistics

For physiological measurements such as body weight and bodyweight change, values are indicated as mean ± SEM (n=8 mice/group). Significance is based on two-way ANOVA with Tukey's post-hoc test. P-value <0.05 was considered statistically significant. For physiological measurements, such as fasting blood glucose, ketone levels, values are indicated as mean ± SEM (n=8 mice/group). Significance is based on two-tailed paired T-test. P-value <0.05 was considered statistically significant. The statistics for these comparisons were conducted using the GraphPad Prism software programme. For proteome analyses, protein validation FDR threshold was 0.01. Pairwise comparisons against the AL control group were performed, with statistical significance assessed using the Benjamini-Hochberg procedure to control the false discovery rate (FDR), applying an adjusted p-value threshold of <0.05. For function enrichment analysis, GO terms and KEGG pathways with a q-value < 0.05 were considered significantly enriched among DEPs, indicating potential functional relevance. For gene set enrichment analysis (GSEA), the proteomic dataset with curated mouse GO biological processes and pathway databases FDR was controlled at 0.05. Gene set similarity was set as p-value < 0.01, and the EnrichmentMap plugin (v3.5.0) in Cytoscape (v3.10) was used to visualize overlapping gene sets and interpret enriched pathways. Network visualization was performed using the STRING plugin (version 2.2.0) implemented in Cytoscape with a confidence score> 0.8. For transcriptome data, differential expression analysis of the quantified transcripts was performed using DESeq2 R Package v.1.20.1. Those transcripts with p-value <0.05 were considered to be significantly differentially expressed among the different categories. For these significant genes, functional enrichment based on GO terms and associated KEGG pathways were inferred based on adjusted p-values <0.05 as implemented in clusterProfiler v3.8.1.

Results and Discussion

Male C57BL/6 mice were fed a normal chow diet and randomly assigned to AL or daily IF16 schedules beginning at 6 weeks of age. The study design, including the timing of experimental interventions and blood and tissue collections, is summarized in Supplementary Figure **(Figure**

S1A). To determine the extent to which 8-hour IF affects energy metabolism, we measured the blood glucose, HbA1c, ketone and cholesterol levels, and body weight of all mice during the four-month dietary intervention period. Mice in the AL group exhibited a trend towards increased blood glucose and HbA1c levels. In contrast, mice in the IF group exhibited a significant decrease in blood glucose and HbA1c levels (**Figure S1B**). IF mice exhibited blood ketone levels that were two- to threefold greater than mice in the AL group (**Figure S2C**). In addition, IF mice exhibited lower blood cholesterol levels compared to AL (**Figure S1D**). IF animals exhibited significantly lower body weight and body weight changes compared to AL mice during the four-month dietary intervention period (**Figure S1F and G**).

Proteomic Profiling

To gain a comprehensive understanding of the mechanisms affected by IF in the liver, muscle, and brain, we performed proteome profiling of these tissues using at least seven biological replicates from each dietary group (AL = 7, IF = 7) (**Figure 1**). Mass spectrometry-based quantitative proteomics analysis of these tissues identified a total of 4,777 proteins in the liver (**Figure 1B and Table S1**). Of these, 835 proteins (17.5%) were differentially expressed in IF tissues compared to the control AL group (**Figure 1A and Table S1**). In muscle, we identified 2,709 proteins, with 155 (5.7%) showing differential expression in IF tissues (**Figure 1C, D and Table S2**). In the cerebral cortex, we identified 6,332 proteins, of which 294 (6%) were differentially expressed in IF tissues (**Figure 1E, F and Table S3**). We next analysed the DEPs across all organs to assess their biological significance.

In the liver, IF led to the upregulation of 446 proteins, predominantly associated with metabolic pathways. These pathways exhibited a >10-fold enrichment in key processes such as the citrate cycle, glycan degradation, butanoate metabolism, glycine, serine, and threonine metabolism, and fatty acid metabolism, among others (**Figure 1G**). Enhancement of these pathways in response to IF may optimize energy metabolism: the citrate cycle is activated to efficiently oxidize fatty acids and generate ATP, while glycan degradation facilitates the conversion of stored glycans into readily usable sugars. Additionally, increased butanoate metabolism enables the liver to utilize short-chain fatty acids, enhancing its adaptation to fasting conditions (Zhou et al., 2017). Interestingly, proteins involved in thermogenesis were also upregulated. Conversely, IF resulted in the downregulation of 389 proteins in the liver, with enrichment observed in pathways such as steroid synthesis and linoleic acid metabolism, alongside other biosynthetic processes (**Figure 1H**). This likely reflects the liver's prioritization of energy-

producing pathways over steroid hormone synthesis during fasting (Seoane-Collazo et al., 2018). Metabolic switching and altered signaling pathways under IF conditions may suppress enzymes involved in steroidogenesis (Grasfeder et al., 2009). This metabolic shift underscores the liver's ability to maintain energy balance and metabolic flexibility in response to limited nutrient availability, highlighting the adaptive mechanisms driven by IF (Smith et al., 2018).

Among the 69 proteins upregulated in skeletal muscle in response to IF, pathways such as pyruvate metabolism, fatty acid biosynthesis, and carbon and fatty acid metabolism exhibited over 20-fold enrichment in IF-fed animals compared to AL-fed controls (**Figure 1I**). This upregulation suggests that IF enhances the muscle's capacity for energy production and substrate utilization, particularly through the activation of metabolic pathways critical for processing pyruvate and synthesizing fatty acids. Additionally, key bioenergetic pathways, including AMPK, PPAR, insulin, and glucagon signaling were upregulated, perhaps indicating that IF promotes metabolic efficiency in muscle by enhancing energy sensing, lipid metabolism, and glucose homeostasis. Conversely, IF led to the downregulation of 86 proteins in muscle, which were primarily associated with pathways such as the citrate cycle, oxidative phosphorylation, thermogenesis, and carbon metabolism (**Figure 1J**). This downregulation may reflect a shift in metabolic priorities, as muscle reduces its reliance on mitochondrial oxidative pathways during fasting periods. Instead, the muscle appears to prioritize alternative energy-generating processes, such as glycolysis and fatty acid oxidation, to adapt to the intermittent nutrient availability imposed by IF.

Notably, muscle's response to IF differs significantly from that of the liver, highlighting tissue-specific adaptations to fasting and feeding cycles. While the liver predominantly upregulates pathways involved in gluconeogenesis, glycan degradation, and fatty acid oxidation, muscle appears to fine-tune its metabolic machinery to balance energy production and substrate utilization in a distinct manner. These findings underscore the organ-specific effects of IF, revealing how different tissues coordinate their metabolic responses to optimize energy balance and physiological function under restricted feeding conditions.

Unlike the liver and muscle, 121 upregulated proteins in the cerebral cortex were primarily linked to metabolic pathways (**Figure 1K**). In contrast, 173 proteins were downregulated in the cerebral cortex, with significant associations observed in pathways such as nucleocytoplasmic transport, calcium signaling, and processes related to neurodegeneration

(**Figure 1L**). These findings highlight the distinct metabolic and functional adaptations of the cortex to IF, which differ markedly from those observed in the liver and muscle.

Identification of Altered Proteins and Metabolic Pathway Dynamics

To investigate the major metabolic and signaling pathways responsive to IF in the liver, cerebral cortex, and muscle, we further analyzed DEPs in these tissues. Notably, the liver exhibited the highest number of DEPs (**Figure 2A, Table S4**), which are primarily involved in metabolic processes. In contrast, fewer changes were observed in muscle (**Figure 2B, Table S4**) and the cerebral cortex (**Figure 2C, Table S4**). In response to IF, the liver exhibits upregulation of several proteins that are intricately involved in key metabolic pathways (**Figure 2A**). Proteins such as PDK2, PDHB, and MECR play critical roles in mitochondrial energy metabolism, including pyruvate metabolism and fatty acid oxidation, which are essential for maintaining energy homeostasis during fasting (Luo et al., 2022; Jiang et al., 2023; Qian et al., 2020). Enzymes like ACADL, DECR1, and BDH1 are directly involved in lipid metabolism, facilitating the breakdown and utilization of fatty acids as an energy source (Diekman et al., 2021; Mäkelä et al., 2019; Williams et al., 2024). Additionally, CTH, CES1C, and GSTMs (e.g., GSTM2, GSTM3) contribute to detoxification and antioxidant pathways, protecting the liver from oxidative stress induced by metabolic shifts (Katsouda et al., 2023; Gan et al 2023; Fafián et al., 2020). Proteins such as GPX3, FDXR, and AKR1B1 further support redox balance and stress response mechanisms (Wu et al., 2023; Mohibi et al., 2024; Yu et al., 2024). Meanwhile, FABP5, PCYT1A, and LPIN2 are associated with lipid transport and phospholipid biosynthesis, ensuring proper lipid handling and membrane integrity (Seo et al., 2020; Haider et al., 2018; Zhang et al., 2019). Finally, HEXA, CTBS, and GUSB are linked to glycosphingolipid and carbohydrate metabolism, highlighting the liver's role in managing glucose and glycoconjugate processing during fasting (Montgomery et al., 2023; Persichetti et al., 2012; Bramwell et al., 2015). In response to IF, the downregulation of key proteins in the liver reflects a shift in metabolic priorities and reduced activity in specific pathways. For instance, CYP450 enzymes such as CYP2E1, CYP3A13, and CYP7B1 are involved in xenobiotic metabolism and bile acid synthesis, suggesting a potential reduction in detoxification processes during fasting (Esteves et al., 2021). Similarly, ACACA and ACACB, key enzymes in fatty acid synthesis, are downregulated, aligning with the suppression of lipogenesis when energy intake is limited (Dong et al., 2024; Bhattacharjee et al., 2020). Proteins like HMGCS1 and FDFT1, which are critical for cholesterol biosynthesis, also show reduced expression, indicating a slowdown in sterol production (Qin et al., 2024; Ha et al.,

2020). Additionally, PFKL, a regulator of glycolysis, is downregulated, reflecting a decreased reliance on glucose metabolism during fasting (Meng et al., 2024). The downregulation of FADS1 and ACSL1, involved in fatty acid desaturation and activation, further highlights a shift away from lipid processing and storage (Reynolds et al., 2020; Wang et al., 2024).

The downregulation of key proteins in muscle tissue reflects a shift in metabolic activity and energy utilization (**Figure 2B**). For instance, DLD and IDH3A/IDH3B are crucial components of the TCA cycle, suggesting a reduction in mitochondrial oxidative metabolism during fasting (Capitanio et al., 2017; Liu et al., 2020). Similarly, GOT1, which plays a role in amino acid metabolism and the malate-aspartate shuttle, is downregulated, indicating a potential decrease in amino acid catabolism and nitrogen handling (Sun et al., 2019).

The upregulation of key proteins in the cerebral cortex highlights adaptive changes in metabolic and signaling pathways (**Figure 2C**). PRKAA1, a subunit of AMPK, is upregulated, indicating enhanced cellular energy sensing and regulation, which promotes energy conservation and catabolic processes (Yang et al., 2020). HMGCS2, a critical enzyme in ketogenesis, suggests an increased production of ketone bodies, providing an alternative energy source for the brain during fasting (Asif et al., 2022). LPCAT2 and PAFAH1B2, involved in phospholipid metabolism and inflammatory signaling, respectively, may play roles in maintaining membrane integrity and modulating neuroinflammatory responses (Cotte et al., 2018; Sudarov et al., 2018). Additionally, PAM and CPE are associated with neuropeptide processing, potentially influencing neuronal signaling and stress adaptation (Powers et al., 2021; Chen et al., 2023). In response to IF, the downregulation of key proteins in the cortex reflects a shift in metabolic and signaling pathways to adapt to reduced nutrient availability. ACSL6 and SLC27A4, involved in fatty acid activation and transport, respectively, show reduced expression, suggesting a decrease in lipid metabolism and utilization in the cortex during fasting (Fernandez et al., 2021; Anderson et al., 2013). LIPE and LIPA, which play roles in lipid hydrolysis and cholesterol metabolism, are also downregulated, indicating a suppression of lipolytic and sterol-related processes (Adom et al.,2024; Arnaboldi et al., 2020). CES1C, an enzyme involved in ester hydrolysis, further supports the downregulation of lipid metabolism pathways (Gan et al., 2023). Additionally, PTDSS2, associated with phospholipid synthesis, is reduced, pointing to a slowdown in membrane lipid production (Yang et al., 2019).

The liver undergoes significant changes in signaling pathways mediated by the upregulation and downregulation of key proteins (**Figure 2D, Table S5**) in response to IF. Upregulated proteins such as NUCB2 and PRKCA play roles in calcium signaling and cellular stress responses, potentially enhancing adaptive mechanisms to maintain energy homeostasis (Liu et al., 2020; Wang et al., 2017). LONP1, a mitochondrial protease, supports protein quality control and metabolic efficiency, while DAXX and PIN1 are involved in apoptosis regulation and cell cycle signaling, respectively, suggesting a balance between cell survival and stress adaptation (Zhao et al., 2022; Tang et al., 2020; Chen et al., 2018). On the other hand, downregulated proteins like FKBP4 and USP47, which are associated with steroid receptor signaling and protein stabilization, indicate a reduction in steroid hormone activity and protein turnover (Kageyama et al., 2021; Lei et al., 2021). UBE3A and RPS12, linked to ubiquitin-mediated degradation and ribosomal function, reflect a slowdown in protein synthesis and degradation pathways (Avagliano et al., 2021; Kale et al., 2018). Additionally, the downregulation of RHOA, PID1, and NCK1, which regulate cytoskeletal dynamics and cell signaling, points to reduced cellular motility and signaling activity (Li et al., 2012; Yang et al., 2023; Li et al., 2014).

The upregulation and downregulation of specific proteins in muscle tissue reflect adaptive changes in signaling pathways to optimize energy utilization and cellular function in response to IF (**Figure 2E, Table S5)**. Upregulated proteins such as CCNY and CSNK2A1 are involved in cell cycle regulation and phosphorylation-dependent signaling, suggesting enhanced cellular repair and stress adaptation mechanisms (Opacka et al., 2023; Yang et al., 2023). ENO1, a key glycolytic enzyme, indicates a potential shift in energy metabolism to maintain ATP production under nutrient scarcity (Huppertz et al., 2022). CCAR2 and KRT6A are associated with DNA damage response and cytoskeletal integrity, respectively, highlighting the muscle's efforts to maintain structural stability and genomic fidelity during fasting (Iyer et al., 2022; Rorke et al., 2015). Conversely, the downregulation of CD44, a cell surface glycoprotein involved in cell adhesion and signaling, suggests reduced inflammatory signaling and cellular interactions, which may help conserve energy and minimize unnecessary cellular activity (Wolf et al., 2020).

The cerebral cortex exhibits adaptive changes in signaling pathways mediated by the upregulation and downregulation of key proteins, many of which contribute to beneficial neuroprotective and metabolic effects (**Figure 2F, Table S5)**. Upregulated proteins such as

PRKAA1 enhance energy sensing and promote cellular resilience by activating pathways that support mitochondrial function and energy efficiency (Yang et al., 2018). MAP2K1 supports cell survival and growth signaling (Mizuno et al., 2023). NOL3 and TNS2 are involved in anti-apoptotic signaling and cytoskeletal organization, respectively, further promoting neuronal stability and repair (Wu et al., 2024; Cheng et al., 2018). Conversely, the downregulation of proteins such as PRKCB and USP8 reduces inflammatory and stress-related signaling, while SLC27A4 and GPRC5B indicate a shift away from lipid metabolism and non-essential signaling (Griss et al., 2019; Zhao et al., 2020; Maekawa et al., 2015; Kim et al., 2018).

To better understand how metabolic protein networks are restructured in response to IF, we compiled protein-protein interactions (PPIs) for all IF-responsive proteins and investigated their functional interplay in the liver (**Figure 2G–J**) and muscle (**Figure 2K–M**). Our analysis identified closely associated protein networks those are associated with fatty acid metabolism in the liver and analyzed their expression levels in response to IF (**Figure 2I and J**). IF induces significant metabolic adaptations in muscle tissue, as revealed by the upregulation and downregulation of key proteins identified through PPI/KEGG networks. Upregulated proteins such as PGD, TKT, FASN, ACLY, ACACA, MAT2A, ENO1, and GCLM highlight a shift toward enhanced lipid metabolism, redox balance, and stress protection (Wakai et al., 2017; Tian et al., 2020; Schroeder et al., 2021; Lin et al., 2013; Luo et al., 2022; Krejsa et al., 2010). PGD and TKT support NADPH production, while FASN, ACLY, and ACACA drive fatty acid synthesis, reflecting a response to energy fluctuations (Currie et al., 2023; TeSlaa et al., 2023). MAT2A and GCLM indicate increased methionine metabolism and glutathione synthesis, safeguarding against oxidative stress, while ENO1 underscores the persistence of glucose metabolism (Cheng et al., 2024). Conversely, downregulated proteins like IDH3B, FH, DLD, NDUFV1, COX4I1, IVD, and CKMT2, involved in the TCA cycle and mitochondrial energy production, suggest a reduced reliance on oxidative metabolism as muscle tissue conserves energy and prioritizes alternative fuel sources (Zhu et al., 2022; Solaimuthu et al., 2022; Fuhrmann et al., 2017; Čunátová et al., 2021; Lin et al., 2024). Together, these changes illustrate a coordinated metabolic shift, balancing energy production, lipid utilization, and stress responses to maintain homeostasis during fasting. This dynamic adaptation underscores the metabolic flexibility of muscle tissue and provides valuable insights into the molecular mechanisms underlying IF.

Furthermore, we have identified additional metabolic and bioenergetic networks modulated by IF across different tissues. In the liver (**Figure S2**), these networks include FGF and insulin signaling, glutamate metabolism, and nucleoside diphosphate metabolic processes, highlighting the liver's central role in energy regulation and metabolic homeostasis. In muscle (**Figure S3**), processes such as biosynthesis and protein glycosylation were prominent, reflecting tissue-specific adaptations to nutrient availability. In the cortex (**Figure S4**), pathways related to brain development, neurotransmitter transport, synaptic vesicle maturation, and cytoskeleton organization were observed, underscoring the brain's adaptive responses to fasting. Collectively, these findings demonstrate the systemic impact of IF, revealing tissue-specific metabolic reprogramming that supports energy conservation, cellular maintenance, and functional adaptation.

Identification of Shared and Tissue-Specific Biological Processes

While the health benefits of IF are well documented, the underlying molecular mechanisms driving these effects remain poorly understood, particularly whether they are mediated through shared or tissue-specific pathways. To address this knowledge gap, we conducted a comparative analysis to identify unique and shared biological processes across the liver, muscle, and cortex in response to IF. First, we compared all proteins expressed in the IF groups across the liver, muscle, and cerebral cortex, identifying 1,997 proteins commonly expressed in response to IF (**Figure 3A**). Next, to elucidate the shared and tissue-specific mechanisms of IF, we focused on DEPs that showed significant changes compared to the AL control group (**Figure 3B**). Our analysis revealed that Serpin A1c was the only protein commonly dysregulated across all three organs, suggesting a potentially central role for this protein in the systemic response to IF. The observation that Serpin A1c levels increase in the liver but decrease in muscle and cerebral cortex in response to IF suggests a tissue-specific regulatory role for this protein during metabolic adaptation IF (**Figure 3C**). In the liver, the upregulation of Serpin A1c, a serine protease inhibitor, may reflect a protective mechanism to modulate inflammation or protein degradation as the body shifts toward fat metabolism and ketogenesis during fasting (Okagawa et al., 2024). Conversely, its reduction in muscle and cerebral cortex could indicate a reduced need for protease inhibition in these tissues, possibly to facilitate protein breakdown for energy or to conserve resources under fasting conditions (Sanfeliu et al., 2019; Pattamaprapanont et al., 2024). These differential responses highlight how IF can trigger distinct molecular adjustments across tissues, reflecting their unique metabolic demands and contributions to whole-body homeostasis. To further validate this finding, we performed

immunohistochemistry to assess Serpin A1c expression in liver tissues obtained from both IF and AL fed animals. The results confirmed that IF upregulates the expression levels of Serpin A1c in the liver (**Figure 3D**).

Next, we conducted an organ-to-organ comparison to identify common DEPs in response to IF. Between the liver and muscle, we identified 25 proteins that were differentially expressed (**Figure 3E**). Notably, LMNB2 (involved in nuclear envelope integrity and cell cycle regulation) (Ji et al., 2022), PC (a key enzyme in gluconeogenesis and anaplerosis) (Hughey et al., 2019), and CTBS (associated with lysosomal function and glycoprotein metabolism) (Yadati et al., 2020) were upregulated in both organs, suggesting their roles in supporting metabolic adaptation and cellular homeostasis during fasting. In contrast, SDHC (a subunit of mitochondrial complex II, critical for the electron transport chain) (Bandara et al., 2021) was downregulated in both tissues, potentially reflecting a reduction in oxidative phosphorylation to conserve energy under nutrient scarcity. The remaining common DEPs exhibited opposing expression patterns, highlighting distinct, organ-specific responses to IF.

Between the liver and cerebral cortex, we identified 33 proteins that were differentially expressed in response to IF (**Figure 3F**). Among the upregulated proteins, CIRBP (involved in stress response and RNA stabilization) (Zhu et al., 2024), UROD (essential for heme biosynthesis) (Nilsson et al., 2009), SCO2 (critical for mitochondrial function and energy production) (Sung et al., 2010), NAPRT (a key enzyme in NAD+ biosynthesis) (Carreira et al., 2023), MRPL13 (involved in mitochondrial protein synthesis) (Cámara et al., 2011), RPS21 (essential for protein translation) (Dinh et al., 2021), PMPCB (crucial for mitochondrial protein import) (Michaelis et al., 2022), and HMGCS2 (a rate-limiting enzyme in ketogenesis) (Kim et al., 2019) were upregulated in both organs. Upregulation of these proteins collectively suggests enhanced stress resilience, mitochondrial function, and metabolic adaptation during fasting. Among the downregulated proteins, RUSF1 (implicated in cell signaling) (Huttlin et al., 2010), LIPA (involved in lipid metabolism) (Lettieri et al., 2013), XPO7 (associated with nuclear transport) (Aksu et al., 2018), and AGPAT3 (involved in phospholipid biosynthesis) (Zhou et al., 2024) were reduced, potentially reflecting a shift in energy utilization and cellular homeostasis. These findings highlight the coordinated yet distinct responses of the liver and cerebral cortex to IF, emphasizing the interplay between shared and tissue-specific mechanisms in metabolic reprogramming. The remaining shared DEPs displayed divergent expression profiles, underscoring the tissue-specific adaptations that occur in response to IF.

Among the 12 DEPs identified between the cortex and muscle in response to IF (**Figure 3G**), PRXL2A (involved in oxidative stress response) (Chen et al., 2019), UBE2M (critical for protein ubiquitination and degradation) (Zhou et al., 2018), and AIMP1 (associated with inflammation and angiogenesis) (Zhou et al., 2020) were upregulated. Upregulation of these proteins suggests enhanced cellular stress resilience, protein homeostasis, and regulatory signaling in both tissues during fasting. Conversely, the downregulated proteins included DES (essential for muscle structural integrity) (Agnetti et al., 2022), MPC2 (crucial for pyruvate transport and energy metabolism) (Pujol et al., 2023), SERPINA1B (involved in protease inhibition and inflammation) (Bidooki et al., 2023), and SERPINA1E (also implicated in protease regulation) (Zhang et al., 2022). The reduction of these proteins may reflect tissue-specific adaptations, such as altered structural maintenance in muscle and modulated inflammatory responses in the cortex. These findings highlight the distinct yet coordinated molecular mechanisms underlying tissue-specific responses to IF.

We also compared the expression levels of all common DEPs in response to IF relative to AL feeding across the liver, muscle, and cerebral cortex to identify the organs in which these proteins were most highly regulated (**Figure S5**). Additionally, we analyzed the common biological processes modulated by IF across all three tissues. Intriguingly, synaptic vesicle localization was the only biological process shared among the liver, muscle, and cortex (**Figure 3H**). This finding suggests a potential role for synaptic vesicle regulation in the systemic adaptation to IF, possibly linking metabolic changes to neuronal regulation of peripheral organs. Although the liver and muscle are not traditionally associated with synaptic function, this conserved process may indicate a broader, unifying neural mechanisms underlying organ responses to nutrient stress.

Analysis of RNA-Protein Concordance

Having established that IF modulates the proteome in the liver, muscle, and cortex, we next investigated the transcriptome to explore IF-induced effects in these organs. To this end, we performed RNA-seq-based transcriptome profiling across all tissues and compared the differentially expressed transcripts with their corresponding proteomic profiles. To further elucidate the integrated proteomic and transcriptomic responses to IF, we analyzed 176 upregulated genes/proteins in the liver (**Figure 4A and B; Figure S6A and B**). These were predominantly associated with metabolic processes, including lipid metabolism,

gluconeogenesis, and amino acid catabolism, reflecting the liver's central role in metabolic adaptation during nutrient scarcity. Similarly, analysis of 146 downregulated genes/proteins revealed their involvement in key pathways such as steroid hormone synthesis, signaling cascades (e.g., PPAR signaling), and inflammatory regulation (**Figure 4C and D; Figure S6C and D**).

A similar integrative analysis in muscle tissue identified 25 upregulated genes/proteins, which were primarily associated with critical metabolic pathways, including fructose and mannose metabolism, the pentose phosphate pathway, fatty acid metabolism, pyruvate metabolism, carbon metabolism, fatty acid biosynthesis, the citrate cycle (TCA cycle), and the AMPK signaling pathway (**Figure 4E and F; Figure S7A and B**). These findings further suggest that IF enhances metabolic flexibility in muscle, promoting energy production and substrate utilization to meet the demands of nutrient scarcity. In contrast, analysis of 31 downregulated genes/proteins highlighted their association with reactive oxygen species (ROS)-related processes and various disease-associated pathways regulation (**Figure 4G and H; Figure S7C and D**). The downregulation of these genes may reflect a protective mechanism to reduce oxidative stress and mitigate the risk of metabolic dysfunction during fasting.

Integrative analysis in the cortex identified 11 upregulated and 14 downregulated genes/proteins in response to IF. The upregulated genes/proteins were enriched in pathways such as autophagy, cell adhesion, PPAR signaling, and metabolic processes. The upregulation of autophagy suggests enhanced cellular clearance and maintenance, while increased PPAR signaling points to improved lipid metabolism and anti-inflammatory responses (**Figure 4I and J; Figure S8A and B**). Upregulated metabolic pathways further indicate a shift toward energy efficiency and utilization of alternative substrates during nutrient scarcity. Conversely, the downregulated genes/proteins were associated with pathways including TGF-beta signaling, p53 signaling, and biosynthesis processes (**Figure 4K and L; Figure S8C and D**). The suppression of TGF-beta and p53 signaling may reflect a reduction in cellular stress and apoptosis, while downregulation of biosynthesis pathways likely represents a conservation of resources during fasting.

While the integration of transcriptomic and proteomic data revealed that only a fraction of expressed genes matched with DEPs, this observation is not unexpected. Our proteomic analysis identified up to a few thousand proteins, whereas transcriptomic profiling detected

over 20,000 genes, highlighting the inherent disparity in the depth and coverage of these two approaches. Additionally, post-transcriptional regulatory mechanisms, such as mRNA stability, translational efficiency, and protein degradation, likely contribute to this discrepancy. This phenomenon, often referred to as "post-transcriptional buffering," means that not all transcripts are translated into proteins, and the correlation between mRNA and protein levels is often modest. These findings underscore the complexity of gene expression regulation and emphasize the importance of multi-omics integration to fully capture the molecular adaptations induced by IF.

Conclusion

This comprehensive study elucidates shared and tissue-specific IF-triggered metabolic adaptations across the liver, muscle, and cerebral cortex. Through integrated proteomic and transcriptomic analyses, we identified both shared and organ-specific responses to IF, revealing a complex interplay of molecular mechanisms that optimize energy utilization, enhance metabolic flexibility, and promote cellular resilience under nutrient scarcity. In the liver, IF caused upregulation of pathways involved in gluconeogenesis, fatty acid oxidation, and ketogenesis, while downregulating biosynthetic processes such as steroid hormone synthesis and cholesterol metabolism. These changes underscore the liver's central role in maintaining systemic energy homeostasis during fasting. Similarly, skeletal muscle exhibited enhanced metabolic efficiency through the upregulation of pathways like pyruvate metabolism, fatty acid biosynthesis, and AMPK signaling, while downregulating oxidative phosphorylation and thermogenesis, reflecting a shift toward alternative energy-generating processes. In the cerebral cortex, IF induced adaptive changes in autophagy, PPAR signaling, and metabolic pathways, while suppressing stress-related and biosynthetic processes, highlighting the brain's unique response to fasting.

Notably, our findings reveal that while some molecular responses to IF are conserved across tissues, such as the upregulation of Serpina1C in the liver and its downregulation in muscle and cortex, others are highly tissue-specific. This divergence underscores the importance of organ-specific metabolic reprogramming in mediating the systemic effects of IF. Furthermore, the identification of synaptic vesicle localization as a shared biological process across all three tissues suggests a novel, unifying mechanism linking metabolic changes to cellular communication and stress adaptation. Despite the observed discordance between

transcriptomic and proteomic data, attributed to post-transcriptional buffering and the inherent limitations of proteomic coverage, our multi-omics approach provides a robust framework for understanding the molecular underpinnings of IF. These insights not only advance our understanding of the physiological adaptations to fasting but also highlight potential therapeutic targets for metabolic disorders, neurodegenerative diseases, and aging. Future studies should explore the functional roles of key proteins and pathways identified here, as well as the long-term implications of IF on tissue health and systemic metabolism.

References

Adom MA, Hahn WN, McCaffery TD, Moors TE, Zhang X, Svenningsson P, et al. Reducing the lipase LIPE in mutant α-synuclein mice improves Parkinson-like deficits and reveals sex differences in fatty acid metabolism. Neurobiol Dis. 2024;199:106593.

Agnetti G, Herrmann H, Cohen S. New roles for desmin in the maintenance of muscle homeostasis. Febs j. 2022;289(10):2755-70.

Aksu M, Pleiner T, Karaca S, Kappert C, Dehne HJ, Seibel K, et al. Xpo7 is a broad-spectrum exportin and a nuclear import receptor. J Cell Biol. 2018;217(7):2329-40.

Anderson CM, Stahl A. SLC27 fatty acid transport proteins. Mol Aspects Med. 2013;34(2-3):516-28.

Anton SD, Moehl K, Donahoo WT, Marosi K, Lee SA, Mainous AG, 3rd, et al. Flipping the Metabolic Switch: Understanding and Applying the Health Benefits of Fasting. Obesity (Silver Spring). 2018;26(2):254-68.

Arnaboldi L, Ossoli A, Giorgio E, Pisciotta L, Lucchi T, Grigore L, et al. LIPA gene mutations affect the composition of lipoproteins: Enrichment in ACAT-derived cholesteryl esters. Atherosclerosis. 2020;297:8-15.

Arumugam TV, Alli-Shaik A, Liehn EA, Selvaraji S, Poh L, Rajeev V, et al. Multiomics analyses reveal dynamic bioenergetic pathways and functional remodeling of the heart during intermittent fasting. Elife. 2023;12.

Asif S, Kim RY, Fatica T, Sim J, Zhao X, Oh Y, et al. Hmgcs2-mediated ketogenesis modulates high-fat diet-induced hepatosteatosis. Mol Metab. 2022;61:101494.

Asif S, Morrow NM, Mulvihill EE, Kim KH. Understanding Dietary Intervention-Mediated Epigenetic Modifications in Metabolic Diseases. Front Genet. 2020;11:590369.

Avagliano Trezza R, Punt AM, Mientjes E, van den Berg M, Zampeta FI, de Graaf IJ, et al. Mono-ubiquitination of Rabphilin 3A by UBE3A serves a non-degradative function. Sci Rep. 2021;11(1):3007.

Bandara AB, Drake JC, Brown DA. Complex II subunit SDHD is critical for cell growth and metabolism, which can be partially restored with a synthetic ubiquinone analog. BMC Molecular and Cell Biology. 2021;22(1):35.

Bhattacharjee K, Nath M, Choudhury Y. Fatty acid synthesis and cancer: Aberrant expression of the ACACA and ACACB genes increases the risk for cancer. Meta Gene. 2020;26:100798.

Bidooki SH, Sánchez-Marco J, Martínez-Beamonte R, Herrero-Continente T, Navarro MA, Rodríguez-Yoldi MJ, et al. Endoplasmic Reticulum Protein TXNDC5 Interacts with PRDX6 and HSPA9 to Regulate Glutathione Metabolism and Lipid Peroxidation in the Hepatic AML12 Cell Line. Int J Mol Sci. 2023;24(24).

Bramwell KK, Mock K, Ma Y, Weis JH, Teuscher C, Weis JJ. β-Glucuronidase, a Regulator of Lyme Arthritis Severity, Modulates Lysosomal Trafficking and MMP-9 Secretion in Response to Inflammatory Stimuli. J Immunol. 2015;195(4):1647-56.

Cámara Y, Asin-Cayuela J, Park Chan B, Metodiev Metodi D, Shi Y, Ruzzenente B, et al. MTERF4 Regulates Translation by Targeting the Methyltransferase NSUN4 to the Mammalian Mitochondrial Ribosome. Cell Metabolism. 2011;13(5):527-39.

Capitanio D, Fania C, Torretta E, Viganò A, Moriggi M, Bravatà V, et al. TCA cycle rewiring fosters metabolic adaptation to oxygen restriction in skeletal muscle from rodents and humans. Sci Rep. 2017;7(1):9723.

Carreira ASA, Ravera S, Zucal C, Thongon N, Irene C, Astigiano C, et al. Mitochondrial rewiring drives metabolic adaptation to NAD(H) shortage in triple negative breast cancer cells. Neoplasia. 2023;41:100903.

Chen H, Boutros PC. VennDiagram: a package for the generation of highly-customizable Venn and Euler diagrams in R. BMC Bioinformatics. 2011;12(1):35.
Chen Y, Wu Y-r, Yang H-y, Li X-z, Jie M-m, Hu C-j, et al. Prolyl isomerase Pin1: a promoter of cancer and a target for therapy. Cell Death & Disease. 2018;9(9):883.
Chen YC, Taylor AJ, Fulcher JM, Swensen AC, Dai XQ, Komba M, et al. Deletion of Carboxypeptidase E in β-Cells Disrupts Proinsulin Processing but Does Not Lead to Spontaneous Development of Diabetes in Mice. Diabetes. 2023;72(9):1277-88.
Chen YF, Wei YY, Yang CC, Liu CJ, Yeh LY, Chou CH, et al. miR-125b suppresses oral oncogenicity by targeting the anti-oxidative gene PRXL2A. Redox Biol. 2019;22:101140.
Cheng L-C, Chen Y-L, Cheng A-N, Lee AY-L, Cho C-Y, Huang J-S, et al. AXL phosphorylates and up-regulates TNS2 and its implications in IRS-1-associated metabolism in cancer cells. Journal of Biomedical Science. 2018;25(1):80.
Cheng S, Li Y, Sun X, Liu Z, Guo L, Wu J, et al. The impact of glucose metabolism on inflammatory processes in sepsis-induced acute lung injury. Front Immunol. 2024;15:1508985.
Cotte AK, Aires V, Fredon M, Limagne E, Derangère V, Thibaudin M, et al. Lysophosphatidylcholine acyltransferase 2-mediated lipid droplet production supports colorectal cancer chemoresistance. Nature Communications. 2018;9(1):322.
Čunátová K, Reguera DP, Vrbacký M, Fernández-Vizarra E, Ding S, Fearnley IM, et al. Loss of COX4I1 Leads to Combined Respiratory Chain Deficiency and Impaired Mitochondrial Protein Synthesis. Cells. 2021;10(2).
Currie E, Schulze A, Zechner R, Walther TC, Farese RV Jr. Cellular fatty acid metabolism and cancer. Cell Metab. 2013;18(2):153-61.
De Silva S, Alli-Shaik A, Gunaratne J. FlexStat: combinatory differentially expressed protein extraction. Bioinformatics Advances. 2024;4(1).
Demichev V, Messner CB, Vernardis SI, Lilley KS, Ralser M. DIA-NN: neural networks and interference correction enable deep proteome coverage in high throughput. Nat Methods. 2020;17(1):41-4.
Diekman EF, van Weeghel M, Suárez-Fariñas M, Argmann C, Ranea-Robles P, Wanders RJA, et al. Dietary restriction in the long-chain acyl-CoA dehydrogenase knockout mouse. Molecular Genetics and Metabolism Reports. 2021;27:100749.
Dinh TTH, Iseki H, Mizuno S, Iijima-Mizuno S, Tanimoto Y, Daitoku Y, et al. Disruption of entire Cables2 locus leads to embryonic lethality by diminished Rps21 gene expression and enhanced p53 pathway. Elife. 2021;10.
Doncheva NT, Morris JH, Gorodkin J, Jensen LJ. Cytoscape StringApp: Network Analysis and Visualization of Proteomics Data. Journal of Proteome Research. 2019;18(2):623-32.
Dong J, Li M, Peng R, Zhang Y, Qiao Z, Sun N. ACACA reduces lipid accumulation through dual regulation of lipid metabolism and mitochondrial function via AMPK- PPARα-CPT1A axis. J Transl Med. 2024;22(1):196.
Esteves F, Rueff J, Kranendonk M. The Central Role of Cytochrome P450 in Xenobiotic Metabolism-A Brief Review on a Fascinating Enzyme Family. J Xenobiot. 2021;11(3):94-114.
Fafián-Labora JA, Rodríguez-Navarro JA, O'Loghlen A. Small Extracellular Vesicles Have GST Activity and Ameliorate Senescence-Related Tissue Damage. Cell Metab. 2020;32(1):71-86.e5.
Fernandez RF, Pereyra AS, Diaz V, Wilson ES, Litwa KA, Martínez-Gardeazabal J, et al. Acyl-CoA synthetase 6 is required for brain docosahexaenoic acid retention and neuroprotection during aging. JCI Insight. 2021;6(11).
Fuhrmann DC, Brüne B. Mitochondrial composition and function under the control of hypoxia. Redox Biology. 2017;12:208-15.

Gan C, Wang J, Wang Y, Martínez-Chávez A, Hillebrand M, de Vries N, et al. Natural deletion of mouse carboxylesterases Ces1c/d/e impacts drug metabolism and metabolic syndrome development. Biomed Pharmacother. 2023;164:114956.
Grasfeder LL, Gaillard S, Hammes SR, Ilkayeva O, Newgard CB, Hochberg RB, et al. Fasting-induced hepatic production of DHEA is regulated by PGC-1alpha, ERRalpha, and HNF4alpha. Mol Endocrinol. 2009;23(8):1171-82.
Griss J, Bauer W, Wagner C, Simon M, Chen M, Grabmeier-Pfistershammer K, et al. B cells sustain inflammation and predict response to immune checkpoint blockade in human melanoma. Nature Communications. 2019;10(1):4186.
Ha NT, Lee CH. Roles of Farnesyl-Diphosphate Farnesyltransferase 1 in Tumour and Tumour Microenvironments. Cells. 2020;9(11).
Haider A, Wei YC, Lim K, Barbosa AD, Liu CH, Weber U, et al. PCYT1A Regulates Phosphatidylcholine Homeostasis from the Inner Nuclear Membrane in Response to Membrane Stored Curvature Elastic Stress. Dev Cell. 2018;45(4):481-95.e8.
Heberle H, Meirelles GV, da Silva FR, Telles GP, Minghim R. InteractiVenn: a web-based tool for the analysis of sets through Venn diagrams. BMC Bioinformatics. 2015;16(1):169.
Hughes CS, Moggridge S, Müller T, Sorensen PH, Morin GB, Krijgsveld J. Single-pot, solid-phase-enhanced sample preparation for proteomics experiments. Nat Protoc. 2019;14(1):68-85.
Hughey CC, Crawford PA. Pyruvate Carboxylase Wields a Double-Edged Metabolic Sword. Cell Metabolism. 2019;29(6):1236-8.
Huppertz I, Perez-Perri JI, Mantas P, Sekaran T, Schwarzl T, Russo F, et al. Riboregulation of Enolase 1 activity controls glycolysis and embryonic stem cell differentiation. Molecular Cell. 2022;82(14):2666-80.e11.
Huttlin EL, Jedrychowski MP, Elias JE, Goswami T, Rad R, Beausoleil SA, et al. A tissue-specific atlas of mouse protein phosphorylation and expression. Cell. 2010;143(7):1174-89.
Iyer DR, Harada N, Clairmont C, Jiang L, Martignetti D, Nguyen H, et al. CCAR2 functions downstream of the Shieldin complex to promote double-strand break end-joining. Proc Natl Acad Sci U S A. 2022;119(49):e2214935119.
Ji J, Li H, Chen J, Wang W. Lamin B2 contributes to the proliferation of bladder cancer cells via activating the expression of cell division cycle-associated protein 3. Int J Mol Med. 2022;50(3).
Jiang C, Lu Y, Zhu R, Zong Y, Huang Y, Wang D, et al. Pyruvate dehydrogenase beta subunit (Pdhb) promotes peripheral axon regeneration by regulating energy supply and gene expression. Experimental Neurology. 2023;363:114368.
Kageyama K, Iwasaki Y, Watanuki Y, Niioka K, Daimon M. Differential Effects of Fkbp4 and Fkbp5 on Regulation of the Proopiomelanocortin Gene in Murine AtT-20 Corticotroph Cells. Int J Mol Sci. 2021;22(11).
Kale A, Ji Z, Kiparaki M, Blanco J, Rimesso G, Flibotte S, et al. Ribosomal Protein S12e Has a Distinct Function in Cell Competition. Dev Cell. 2018;44(1):42-55.e4.
Katsouda A, Markou M, Zampas P, Varela A, Davos CH, Vellecco V, et al. CTH/MPST double ablation results in enhanced vasorelaxation and reduced blood pressure via upregulation of the eNOS/sGC pathway. Front Pharmacol. 2023;14:1090654.
Kim D, Paggi JM, Park C, Bennett C, Salzberg SL. Graph-based genome alignment and genotyping with HISAT2 and HISAT-genotype. Nature Biotechnology. 2019;37(8):907-15.
Kim JT, Li C, Weiss HL, Zhou Y, Liu C, Wang Q, et al. Regulation of Ketogenic Enzyme HMGCS2 by Wnt/β-catenin/PPARγ Pathway in Intestinal Cells. Cells. 2019;8(9).

Kim Y-J, Greimel P, Hirabayashi Y. GPRC5B-Mediated Sphingomyelin Synthase 2 Phosphorylation Plays a Critical Role in Insulin Resistance. iScience. 2018;8:250-66.
Kolde R. pheatmap: Pretty Heatmaps. R package version 1.0.12. 2018. Available from: https://github.com/raivokolde/pheatmap
Krejsa CM, Franklin CC, White CC, Ledbetter JA, Schieven GL, Kavanagh TJ. Rapid activation of glutamate cysteine ligase following oxidative stress. J Biol Chem. 2010;285(21):16116-24.
Lei H, Xu H-Z, Shan H-Z, Liu M, Lu Y, Fang Z-X, et al. Targeting USP47 overcomes tyrosine kinase inhibitor resistance and eradicates leukemia stem/progenitor cells in chronic myelogenous leukemia. Nature Communications. 2021;12(1):51.
Lettieri Barbato D, Tatulli G, Aquilano K, Ciriolo MR. FoxO1 controls lysosomal acid lipase in adipocytes: implication of lipophagy during nutrient restriction and metformin treatment. Cell Death & Disease. 2013;4(10):e861-e.
Li B, Antonyak MA, Zhang J, Cerione RA. RhoA triggers a specific signaling pathway that generates transforming microvesicles in cancer cells. Oncogene. 2012;31(45):4740-9.
Li H, Dusseault J, Larose L. Nck1 depletion induces activation of the PI3K/Akt pathway by attenuating PTP1B protein expression. Cell Communication and Signaling. 2014;12(1):71.
Liao Y, Smyth GK, Shi W. featureCounts: an efficient general purpose program for assigning sequence reads to genomic features. Bioinformatics. 2014;30(7):923-30.
Lin R, Tao R, Gao X, Li T, Zhou X, Guan KL, et al. Acetylation stabilizes ATP-citrate lyase to promote lipid biosynthesis and tumor growth. Mol Cell. 2013;51(4):506-18.
Lin W, Zhou J, Ma Y, Ge L, Luo Y, Wang Y, et al. Prognostic value of mitochondrial CKMT2 in Pan-cancer and its tumor immune correlation analysis. Sci Rep. 2024;14(1):342.
Liu X, Qiao Y, Ting X, Si W. Isocitrate dehydrogenase 3A, a rate-limiting enzyme of the TCA cycle, promotes hepatocellular carcinoma migration and invasion through regulation of MTA1, a core component of the NuRD complex. Am J Cancer Res. 2020;10(10):3212-29.
Liu Y, Chen X, Qu Y, Song L, Lin Q, Li M, et al. Central nesfatin-1 activates lipid mobilization in adipose tissue and fatty acid oxidation in muscle via the sympathetic nervous system. Biofactors. 2020;46(3):454-64.
Longo Valter D, Mattson Mark P. Fasting: Molecular Mechanisms and Clinical Applications. Cell Metabolism. 2014;19(2):181-92.
López-Otín C, Blasco MA, Partridge L, Serrano M, Kroemer G. Hallmarks of aging: An expanding universe. Cell. 2023;186(2):243-78.
Love MI, Huber W, Anders S. Moderated estimation of fold change and dispersion for RNA-seq data with DESeq2. Genome Biology. 2014;15(12):550.
Luo H, Song Y, Zhang J-a, Liu Y, Chen F, Wang Z, et al. MAT2A facilitates PDCD6 methylation and promotes cell growth under glucose deprivation in cervical cancer. Cell Death Discovery. 2022;8(1):176.
Luo Y, Zhou W, Li R, Limbu SM, Qiao F, Chen L, et al. Inhibition of pyruvate dehydrogenase kinase improves carbohydrate utilization in Nile tilapia by regulating PDK2/4-PDHE1α axis and insulin sensitivity. Animal Nutrition. 2022;11:25-37.
Maekawa M, Iwayama Y, Ohnishi T, Toyoshima M, Shimamoto C, Hisano Y, et al. Investigation of the fatty acid transporter-encoding genes SLC27A3 and SLC27A4 in autism. Sci Rep. 2015;5(1):16239.
Mäkelä AM, Hohtola E, Miinalainen IJ, Autio JA, Schmitz W, Niemi KJ, et al. Mitochondrial 2,4-dienoyl-CoA reductase (Decr) deficiency and impairment of thermogenesis in mouse brown adipose tissue. Sci Rep. 2019;9(1):12038.
Mattson MP, Moehl K, Ghena N, Schmaedick M, Cheng A. Intermittent metabolic switching, neuroplasticity and brain health. Nat Rev Neurosci. 2018;19(2):63-80.
Mattson MP. The Intermittent Fasting Revolution. 2022; MIT Press, Cambridge, MA.

Mattson MP. The cyclic metabolic switching theory of intermittent fasting. *Nat Metab.* 2025; doi: 10.1038/s42255-025-01254-5.
Meng Y, Guo D, Lin L, Zhao H, Xu W, Luo S, et al. Glycolytic enzyme PFKL governs lipolysis by promoting lipid droplet–mitochondria tethering to enhance β-oxidation and tumor cell proliferation. Nature Metabolism. 2024;6(6):1092-107.
Merico D, Isserlin R, Stueker O, Emili A, Bader GD. Enrichment map: a network-based method for gene-set enrichment visualization and interpretation. PLoS One. 2010;5(11):e13984.
Michaelis JB, Brunstein ME, Bozkurt S, Alves L, Wegner M, Kaulich M, et al. Protein import motor complex reacts to mitochondrial misfolding by reducing protein import and activating mitophagy. Nature Communications. 2022;13(1):5164.
Mizuno S, Ikegami M, Koyama T, Sunami K, Ogata D, Kage H, et al. High-Throughput Functional Evaluation of MAP2K1 Variants in Cancer. Mol Cancer Ther. 2023;22(2):227-39.
Mohibi S, Zhang Y, Perng V, Chen M, Zhang J, Chen X. Ferredoxin 1 is essential for embryonic development and lipid homeostasis. Elife. 2024;13.
Montgomery MK, Bayliss J, Nie S, de Nardo W, Keenan SN, Anari M, et al. Liver-Secreted Hexosaminidase A Regulates Insulin-Like Growth Factor Signaling and Glucose Transport in Skeletal Muscle. Diabetes. 2023;72(6):715-27.
Nilsson R, Schultz IJ, Pierce EL, Soltis KA, Naranuntarat A, Ward DM, et al. Discovery of genes essential for heme biosynthesis through large-scale gene expression analysis. Cell Metab. 2009;10(2):119-30.
Okagawa S, Sakaguchi M, Okubo Y, Takekuma Y, Igata M, Kondo T, et al. Hepatic SerpinA1 improves energy and glucose metabolism through regulation of preadipocyte proliferation and UCP1 expression. Nat Commun. 2024;15(1):9585.
Opacka A, Żuryń A, Krajewski A, Mikołajczyk K. The role of cyclin Y in normal and pathological cells. Cell Cycle. 2023;22(8):859-69.
Pattamaprapanont P, Cooney EM, MacDonald TL, Paulo JA, Pan H, Dreyfuss JM, et al. Matrisome proteomics reveals novel mediators of muscle remodeling with aerobic exercise training. Matrix Biology Plus. 2024;23:100159.
Persichetti E, Klein K, Paciotti S, Lecointe K, Balducci C, Franken S, et al. Lysosomal di-N-acetylchitobiase-deficient mouse tissues accumulate Man2GlcNAc2 and Man3GlcNAc2. Biochim Biophys Acta. 2012;1822(7):1137-46.
Powers KG, Ma XM, Eipper BA, Mains RE. Cell-type specific knockout of peptidylglycine α-amidating monooxygenase reveals specific behavioral roles in excitatory forebrain neurons and cardiomyocytes. Genes Brain Behav. 2021;20(2):e12699.
Pujol C, Lebigot E, Gaignard P, Galai S, Kraoua I, Bault JP, et al. MPC2 variants disrupt mitochondrial pyruvate metabolism and cause an early-onset mitochondriopathy. Brain. 2023;146(3):858-64.
Qian S, Ma L, Peng S, Xu Y, Wu K, Shen S, et al. ATP reduces mitochondrial MECR protein in liver of diet-induced obese mice in mechanism of insulin resistance. Biosci Rep. 2020;40(6).
Qin P, Zhou P, Huang Y, Long B, Gao R, Zhang S, et al. Upregulation of rate-limiting enzymes in cholesterol metabolism by PKCδ mediates endothelial apoptosis in diabetic wound healing. Cell Death Discovery. 2024;10(1):263.
Rappsilber J, Mann M, Ishihama Y. Protocol for micro-purification, enrichment, pre-fractionation and storage of peptides for proteomics using StageTips. Nat Protoc. 2007;2(8):1896-906.

Reynolds LM, Dutta R, Seeds MC, Lake KN, Hallmark B, Mathias RA, et al. FADS genetic and metabolomic analyses identify the Δ5 desaturase (FADS1) step as a critical control point in the formation of biologically important lipids. Sci Rep. 2020;10(1):15873.
Ritchie ME, Phipson B, Wu D, Hu Y, Law CW, Shi W, et al. limma powers differential expression analyses for RNA-sequencing and microarray studies. Nucleic Acids Research. 2015;43(7):e47-e.
Rorke EA, Adhikary G, Young CA, Rice RH, Elias PM, Crumrine D, et al. Structural and biochemical changes underlying a keratoderma-like phenotype in mice lacking suprabasal AP1 transcription factor function. Cell Death & Disease. 2015;6(2):e1647-e.
Sanfeliu A, Hokamp K, Gill M, Tropea D. Transcriptomic Analysis of Mecp2 Mutant Mice Reveals Differentially Expressed Genes and Altered Mechanisms in Both Blood and Brain. Front Psychiatry. 2019;10:278.
Schroeder B, Vander Steen T, Espinoza I, Venkatapoorna CMK, Hu Z, Silva FM, et al. Fatty acid synthase (FASN) regulates the mitochondrial priming of cancer cells. Cell Death & Disease. 2021;12(11):977.
Seo J, Jeong D-W, Park J-W, Lee K-W, Fukuda J, Chun Y-S. Fatty-acid-induced FABP5/HIF-1 reprograms lipid metabolism and enhances the proliferation of liver cancer cells. Communications Biology. 2020;3(1):638.
Seoane-Collazo P, Roa J, Rial-Pensado E, Liñares-Pose L, Beiroa D, Ruíz-Pino F, et al. SF1-Specific AMPKα1 Deletion Protects Against Diet-Induced Obesity. Diabetes. 2018;67(11):2213-26.
Smith RL, Soeters MR, Wüst RCI, Houtkooper RH. Metabolic Flexibility as an Adaptation to Energy Resources and Requirements in Health and Disease. Endocr Rev. 2018;39(4):489-517.
Solaimuthu B, Lichtenstein M, Hayashi A, Khatib A, Plaschkes I, Nevo Y, et al. Depletion of Fumarate Hydratase, an Essential TCA Cycle Enzyme, Drives Proliferation in a Two-Step Model. Cancers (Basel). 2022;14(22).
Subramanian A, Tamayo P, Mootha VK, Mukherjee S, Ebert BL, Gillette MA, et al. Gene set enrichment analysis: A knowledge-based approach for interpreting genome-wide expression profiles. Proceedings of the National Academy of Sciences. 2005;102(43):15545-50.
Sudarov A, Zhang XJ, Braunstein L, LoCastro E, Singh S, Taniguchi Y, et al. Mature Hippocampal Neurons Require LIS1 for Synaptic Integrity: Implications for Cognition. Biol Psychiatry. 2018;83(6):518-29.
Sun W, Luan S, Qi C, Tong Q, Yan S, Li H, et al. Aspulvinone O, a natural inhibitor of GOT1 suppresses pancreatic ductal adenocarcinoma cells growth by interfering glutamine metabolism. Cell Commun Signal. 2019;17(1):111.
Sung HJ, Ma W, Wang P-y, Hynes J, O'Riordan TC, Combs CA, et al. Mitochondrial respiration protects against oxygen-associated DNA damage. Nature Communications. 2010;1(1):5.
Szklarczyk D, Kirsch R, Koutrouli M, Nastou K, Mehryary F, Hachilif R, et al. The STRING database in 2023: protein–protein association networks and functional enrichment analyses for any sequenced genome of interest. Nucleic Acids Research. 2022;51(D1):D638-D46.
Tang S, Ding S, Yu L, Shen H, Wan Y, Wu Y. Effects of HPV16 E6 protein on Daxx-induced apoptosis in C33A cells. Cellular & Molecular Biology Letters. 2020;25(1):38.
TeSlaa T, Ralser M, Fan J, Rabinowitz JD. The pentose phosphate pathway in health and disease. Nat Metab. 2023;5(8):1275-1289.
Tian N, Liu Q, Li Y, Tong L, Lu Y, Zhu Y, et al. Transketolase Deficiency in Adipose Tissues Protects Mice From Diet-Induced Obesity by Promoting Lipolysis. Diabetes. 2020;69(7):1355-67.

Tyanova S, Temu T, Sinitcyn P, Carlson A, Hein MY, Geiger T, et al. The Perseus computational platform for comprehensive analysis of (prote)omics data. Nature Methods. 2016;13(9):731-40.
Wakai E, Aritake K, Urade Y, Fujimori K. Prostaglandin D(2) enhances lipid accumulation through suppression of lipolysis via DP2 (CRTH2) receptors in adipocytes. Biochem Biophys Res Commun. 2017;490(2):393-9.
Wang CH, Surbhi, Goraya S, Byun J, Pennathur S. Fatty acids and inflammatory stimuli induce expression of long-chain acyl-CoA synthetase 1 to promote lipid remodeling in diabetic kidney disease. J Biol Chem. 2024;300(1):105502.
Wang F, Xu C, Reece EA, Li X, Wu Y, Harman C, et al. Protein kinase C-alpha suppresses autophagy and induces neural tube defects via miR-129-2 in diabetic pregnancy. Nat Commun. 2017;8:15182.
Williams AS, Crown SB, Lyons SP, Koves TR, Wilson RJ, Johnson JM, et al. Ketone flux through BDH1 supports metabolic remodeling of skeletal and cardiac muscles in response to intermittent time-restricted feeding. Cell Metab. 2024;36(2):422-37.e8.
Wolf KJ, Shukla P, Springer K, Lee S, Coombes JD, Choy CJ, et al. A mode of cell adhesion and migration facilitated by CD44-dependent microtentacles. Proc Natl Acad Sci U S A. 2020;117(21):11432-43.
Wu L, Zhu K, Sun Y, Li T, Zhu J, Tong H, et al. Nucleolar protein 3 promotes proliferation of bladder cancer cells through the PI3K-Akt pathway. World Journal of Surgical Oncology. 2024;22(1):316.
Wu X, Tang S, Dai Q, Yi B, Yang S, Sun J, et al. Vitamin D-vitamin D receptor alleviates oxidative stress in ischemic acute kidney injury via upregulating glutathione peroxidase 3. Faseb j. 2023;37(2):e22738.
Yadati T, Houben T, Bitorina A, Shiri-Sverdlov R. The Ins and Outs of Cathepsins: Physiological Function and Role in Disease Management. Cells. 2020;9(7).
Yang B, Zhang J, Wang J, Fan W, Barbier-Torres L, Yang X, et al. CSNK2A1-mediated MAX phosphorylation upregulates HMGB1 and IL-6 expression in cholangiocarcinoma progression. Hepatol Commun. 2023;7(7).
Yang J, Li S, He J, Xu Q, Xie M, Yang C, et al. Dual role of PID1 in regulating apoptosis induced by distinct anticancer-agents through AKT/Raf-1-dependent pathway in hepatocellular carcinoma. Cell Death Discovery. 2023;9(1):139.
Yang Q, Ma Q, Xu J, Liu Z, Zou J, Shen J, et al. Prkaa1 Metabolically Regulates Monocyte/Macrophage Recruitment and Viability in Diet-Induced Murine Metabolic Disorders. Front Cell Dev Biol. 2020;8:611354.
Yang Q, Xu J, Ma Q, Liu Z, Sudhahar V, Cao Y, et al. PRKAA1/AMPKα1-driven glycolysis in endothelial cells exposed to disturbed flow protects against atherosclerosis. Nature Communications. 2018;9(1):4667.
Yang X, Liang J, Ding L, Li X, Lam SM, Shui G, et al. Phosphatidylserine synthase regulates cellular homeostasis through distinct metabolic mechanisms. PLoS Genet. 2019;15(12):e1008548.
Yu G, Wang L-G, Han Y, He Q-Y. clusterProfiler: an R Package for Comparing Biological Themes Among Gene Clusters. OMICS: A Journal of Integrative Biology. 2012;16(5):284-7.
Yu PC, Hou D, Chang B, Liu N, Xu CH, Chen X, et al. SMARCA5 reprograms AKR1B1-mediated fructose metabolism to control leukemogenesis. Dev Cell. 2024;59(15):1954-71.e7.
Zhang P, Csaki LS, Ronquillo E, Baufeld LJ, Lin JY, Gutierrez A, et al. Lipin 2/3 phosphatidic acid phosphatases maintain phospholipid homeostasis to regulate chylomicron synthesis. J Clin Invest. 2019;129(1):281-95.

Zhang Y, Wu X, Xu M, Yue T, Ling P, Fang T, et al. Comparative Proteomic Analysis of Liver Tissues and Serum in db/db Mice. Int J Mol Sci. 2022;23(17).
Zhao J, Bi W, Zhang J, Xiao S, Zhou R, Tsang CK, et al. USP8 protects against lipopolysaccharide-induced cognitive and motor deficits by modulating microglia phenotypes through TLR4/MyD88/NF-κB signaling pathway in mice. Brain, Behavior, and Immunity. 2020;88:582-96.
Zhao K, Huang X, Zhao W, Lu B, Yang Z. LONP1-mediated mitochondrial quality control safeguards metabolic shifts in heart development. Development. 2022;149(6).
Zhou D, Pan Q, Liu XL, Yang RX, Chen YW, Liu C, et al. Clostridium butyricum B1 alleviates high-fat diet-induced steatohepatitis in mice via enterohepatic immunoregulation. J Gastroenterol Hepatol. 2017;32(9):1640-8.
Zhou H, Fick K, Patel V, Hilton LR, Kim HW, Bagi Z, et al. AGPAT3 deficiency impairs adipocyte differentiation and leads to a lean phenotype in mice. Am J Physiol Endocrinol Metab. 2024;327(1):E69-e80.
Zhou W, Xu J, Tan M, Li H, Li H, Wei W, et al. UBE2M Is a Stress-Inducible Dual E2 for Neddylation and Ubiquitylation that Promotes Targeted Degradation of UBE2F. Mol Cell. 2018;70(6):1008-24.e6.
Zhou Z, Sun B, Huang S, Yu D, Zhang X. Roles of aminoacyl-tRNA synthetase-interacting multi-functional proteins in physiology and cancer. Cell Death & Disease. 2020;11(7):579.
Zhu S, Huang J, Xu R, Wang Y, Wan Y, McNeel R, et al. Isocitrate dehydrogenase 3b is required for spermiogenesis but dispensable for retinal viability. J Biol Chem. 2022;298(9):102387.
Zhu X, Guan R, Zou Y, Li M, Chen J, Zhang J, et al. Cold-inducible RNA binding protein alleviates iron overload-induced neural ferroptosis under perinatal hypoxia insult. Cell Death & Differentiation. 2024;31(4):524-39.

Figure Legends – Main Figures

Figure 1. Differential protein expression and functional analysis in response to intermittent fasting across multiple tissues.

(**A**) Heatmap of proteins significantly differentially expressed in IF group and AL group in liver (**A**), in muscle (**C**) and in cerebral cortex (**E**). The color scale denotes z-score normalized protein abundances. Red denotes higher protein abundance, and blue lower protein abundance. (**B**) Volcan plot of all protein expression in IF groups in comparison to the AL group in liver (**B**), in muscle (**D**) and in cerebral cortex (**F**). Each dot represents a protein. Red dots showing protein with $p<0.05$ and $|\log2FC|>1$. Bule dots showing proteins with $p <0.05$ and $0<|\log2FC|<1$. Green dots showing proteins with $p>0.05$ and $|\log2FC>1|$. (**G**) Enrichment analysis of modulated processes and pathways in IF groups in comparison to the AL group in both upregulated and downregulated pathways in liver (**G**,**H**), muscle (**I**, **J**) and cerebral cortex (**K**, **L**). The FDR was controlled at 0.05. Each bar represents a functional process or pathway. Red denotes higher protein abundance, and blue lower protein abundance. n = 7 mice in each group.

Figure 2. Differential expression patterns of proteins, functional analysis, and associated protein networks across multiple tissues in response to intermittent fasting across multiple tissues.

(**A**) Heatmap of significantly different proteins involved in metabolic process in IF group in comparison to AL group in liver (**A**), muscle (**B**) and cerebral cortex (**C**). (**D**) Heatmap of significantly different proteins involved in signaling pathways in IF group in comparison to AL group in liver (**D**), muscle (**E**) and cerebral cortex (**F**). (**G**) Functional transition network that shows metabolic processes (**G**) and fatty acid metabolism (**H, I**) in response to IF in liver and metabolic processes (**K, L**) in response to IF in muscle. (**J**) Heatmap of fatty acid metabolism related protein expression in response to IF in liver. (**M**) Heatmap of metabolic pathways related protein expression in response to IF in muscle. The FDR was controlled at 0.05 for GO biological processes and pathway databases. The functional transition network was based one gene set similarity as p value<0.01. n = 7 mice in each group.

Figure 3. Integrative analysis of protein expression and functional enrichment across multiple tissues.

(**A**) Venn diagram illustrating common proteins shared among the liver, muscle, and cerebral cortex. (**B**) Venn diagram depicting common differentially expressed proteins across the liver, muscle, and cortex. (**C**) Expression levels of Serpina1c in the liver, muscle, and cerebral cortex. (**D**) alpha1-antitrypsin staining in green in the liver of both AL and IF mice. n = 3 mice in each group. (**E**) Heatmap of overlapping differentially expressed proteins between the liver and muscle. (**F**) Heatmap of overlapping differentially expressed proteins between the liver and cerebral cortex. (**G**) Heatmap of overlapping differentially expressed proteins between the cerebral cortex and muscle. (**H**) Venn diagram highlighting common biological processes shared among the liver, muscle, and cerebral cortex. data was presented as mean ± SEM with $p<0.05$ was defined as significantly different. n = 7 mice in each group.

Figure 4. Integrative Analysis of Proteomics and RNA-Sequencing with Functional Enrichment Across Multiple Tissues

(**A**)Venn diagrams illustrate genes with concordant regulation at both the transcript and protein levels. Overlapping up-regulated genes are shown for (**A**) liver, (**E**) muscle, and (**I**) cerebral cortex, with their corresponding KEGG pathway enrichments in (**B**) liver, (**F**) muscle, and (**J**) cerebral cortex. (**C**) Overlapping down-regulated genes are depicted for (**C**) liver, (**G**) muscle, and (**K**) cerebral cortex, with their KEGG pathway enrichments in (**D**) liver, (**H**) muscle, and (**L**) cortex. $p< 0.05$ was defined as significantly difference for KEGG enrichment analysis. n = 7 mice in each group. n= 8 each group for RNA-seq data.

Figure Legends – Supplementary Figures

S. Figure 1. Experimental Design and Metabolic Analysis. A) Male mice were divided into two groups: Ad Libitum (AL) and 16:8 fasting (IF) (n=8 per group). Metabolic parameters measured at termination included: fasting blood glucose (B), HbA1c (C), ketone bodies (D), and total cholesterol (E) (mean ± SEM; two-tailed paired t-test: **p<0.01, ***p<0.001, ****p<0.0001 vs AL). Panels F-G show weekly body weight trajectories and net weight change (mean ± SEM; two-way ANOVA with Tukey's post hoc: *p<0.05, **p<0.01 vs AL).

S. Figure 2. Network mapping of IF-responsive proteins in liver

Protein-protein interaction networks generated using STRING analysis highlight multiple functional pathways associated with proteins differentially expressed in liver in response to intermittent fasting. Red denotes increased expression, and blue denotes decreased expression. n= 7 each group.

S. Figure 3. Network mapping of IF-responsive proteins in muscle

Protein-protein interaction networks generated using STRING analysis highlight multiple functional pathways associated with proteins differentially expressed in muscle in response to intermittent fasting. Red denotes increased expression, and blue denotes decreased expression. n= 7 each group.

S. Figure 4. Network mapping of IF-responsive proteins in cortex

Protein-protein interaction networks generated using STRING analysis highlight multiple functional pathways associated with proteins differentially expressed in cortex in response to intermittent fasting. Red denotes increased expression, and blue denotes decreased expression. n= 7 each group.

S. Figure 5. Shared differentially expressed proteins across organs in response to intermittent fasting.

(**A**) Heatmaps depict differentially expressed proteins common to (**A**) liver and muscle, (**B**) liver and cortex, and (**C**) cortex and muscle. Protein expression levels are represented by colours, corresponding to normalized protein intensities. Red denotes increased expression, and blue denotes decreased expression. n= 7 each group.

S. Figure 6. Integrative analysis of proteomics and RNA-seq data in liver under intermittent fasting.

(**A**) Heatmaps display genes with concordant regulation at both the transcript and protein levels. Genes are categorized based on their response to intermittent fasting: (**A**) up-regulated proteins, (**B**) up-regulated RNAs, (**C**) down-regulated proteins, and (**D**) down-regulated RNAs. Colours represent normalized protein intensities for protein and raw FPKM for RNA. Red denotes increased expression, and blue denotes decreased expression. n= 8 each group for RNA-seq data. n= 7 each group for proteomics data.

S. Figure 7. Integrative analysis of proteomics and RNA-seq data in muscle under intermittent fasting.

(**A**) Heatmaps display genes with concordant regulation at both the transcript and protein levels. Genes are categorized based on their response to intermittent fasting: (**A**) up-regulated proteins, (**B**) up-regulated RNAs, (**C**) down-regulated proteins, and (**D**) down-regulated RNAs. Colours represent normalized protein intensities for protein and raw FPKM for RNA. Red denotes increased expression, and blue denotes decreased expression. n= 8 each group for RNA-seq data. n= 7 each group for proteomics data.

S. Figure 8. Integrative analysis of proteomics and RNA-seq data in cortex under intermittent fasting.

(**A**) Heatmaps display genes with concordant regulation at both the transcript and protein levels. Genes are categorized based on their response to intermittent fasting: (**A**) up-regulated proteins, (**B**) up-regulated RNAs, (**C**) down-regulated proteins, and (**D**) down-regulated RNAs. Colours represent normalized protein intensities for protein and raw FPKM for RNA. Red denotes increased expression, and blue denotes decreased expression. n= 8 each group for RNA-seq data. n= 7 each group for proteomics data.

Abbreviations

AcAc – Acetoacetate
ACACA – Acetyl-CoA Carboxylase Alpha
ACLY – ATP Citrate Lyase
ACN – Acetonitrile
ACSL1 – Acyl-CoA Synthetase Long-Chain Family Member 1
ACSL6 – Acyl-CoA Synthetase Long-Chain Family Member 6
AIMP1 – Aminoacyl tRNA Synthetase Complex-Interacting Multifunctional Protein 1
AL – Ad Libitum (unrestricted feeding)
AMPK – AMP-activated Protein Kinase
BCA – Bicinchoninic Acid Assay
BHB – β-Hydroxybutyrate
CCAR2 – Cell Cycle and Apoptosis Regulator 2
CCNY – Cyclin Y
CD44 – CD44 Molecule
cDNA – Complementary DNA
CES1C – Carboxylesterase 1C
CKMT2 – Creatine Kinase, Mitochondrial 2
COX4I1 – Cytochrome c Oxidase Subunit 4I1
CPE – Carboxypeptidase E
CSNK2A1 – Casein Kinase 2 Alpha 1
CYP2E1 – Cytochrome P450 Family 2 Subfamily E Member 1
CYP3A13 – Cytochrome P450 Family 3 Subfamily A Member 13
CYP450 – Cytochrome P450 (liver-specific enzymes)
CYP7B1 – Cytochrome P450 Family 7 Subfamily B Member 1
DAXX – Death Domain-Associated Protein
DEGs – Differentially Expressed Genes
DEPs – Differentially Expressed Proteins
DES – Desmin
DIA – Data-Independent Acquisition
DLD – Dihydrolipoamide Dehydrogenase
ENO1 – Enolase 1
FADS1 – Fatty Acid Desaturase 1
FASN – Fatty Acid Synthase
FDFT1 – Farnesyl-Diphosphate Farnesyltransferase 1
FDR – False Discovery Rate
FH – Fumarate Hydratase
FKBP4 – FK506 Binding Protein 4
FPKM – Fragments Per Kilobase of transcript per Million mapped reads
GCLM – Glutamate-Cysteine Ligase Modifier Subunit
GO – Gene Ontology
GOT1 – Glutamic-Oxaloacetic Transaminase 1
GPRC5B – G Protein-Coupled Receptor Class C Group 5 Member B
GSEA – Gene Set Enrichment Analysis
HCD – Higher-energy Collisional Dissociation
HMGCS1 – 3-Hydroxy-3-Methylglutaryl-CoA Synthase 1
HMGCS2 – 3-Hydroxy-3-Methylglutaryl-CoA Synthase 2
IDH3B – Isocitrate Dehydrogenase 3 (NAD+) Beta
IF – Intermittent Fasting

IVD – Isovaleryl-CoA Dehydrogenase
KEGG – Kyoto Encyclopedia of Genes and Genomes
KRT6A – Keratin 6A
LC-MS – Liquid Chromatography-Mass Spectrometry
LIPA – Lipase A, Lysosomal Acid Type
LIPE – Lipase E, Hormone Sensitive Type
LONP1 – Lon Peptidase 1, Mitochondrial
LPCAT2 – Lysophosphatidylcholine Acyltransferase 2
MAP2K1 – Mitogen-Activated Protein Kinase Kinase 1
MAT2A – Methionine Adenosyltransferase 2A
MPC2 – Mitochondrial Pyruvate Carrier 2
MS1 – Mass Spectrometry Level 1 (Master Scan)
MS2 – Mass Spectrometry Level 2 (Fragmentation Scan)
NAD+ – Nicotinamide Adenine Dinucleotide
NADPH – Nicotinamide Adenine Dinucleotide Phosphate
NCK1 – NCK Adaptor Protein 1
NDUFV1 – NADH:Ubiquinone Oxidoreductase Core Subunit V1
NOL3 – Nucleolar Protein 3
NUCB2 – Nucleobindin 2
OD – Optical Density
PAFAH1B2 – Platelet-Activating Factor Acetylhydrolase 1B2
PAM – Peptidylglycine Alpha-Amidating Monooxygenase
PFKL – Phosphofructokinase, Liver Type
PID1 – Phosphotyrosine Interaction Domain Containing 1
PIN1 – Peptidylprolyl Isomerase NIMA-Interacting 1
PPAR – Peroxisome Proliferator-Activated Receptor
PPI – Protein-Protein Interaction
PRKAA1 – Protein Kinase AMP-Activated Catalytic Subunit Alpha 1
PRKCA – Protein Kinase C Alpha
PRKCB – Protein Kinase C Beta
PRXL2A – Peroxiredoxin-Like 2A
PTDSS2 – Phosphatidylserine Synthase 2
RHOA – Ras Homolog Family Member A
RNA-seq – RNA Sequencing
ROS – Reactive Oxygen Species
RPS12 – Ribosomal Protein S12
SERPINA1B – Serpin Family A Member 1B
SERPINA1E – Serpin Family A Member 1E
SLC27A4 – Solute Carrier Family 27 Member 4
TCA cycle – Tricarboxylic Acid Cycle (Citric Acid Cycle)
TCEP – Tris(2-carboxyethyl)phosphine
TFA – Trifluoroacetic Acid
TGF-beta – Transforming Growth Factor-beta
TNS2 – Tensin 2
UBE2M – Ubiquitin Conjugating Enzyme E2 M
UBE3A – Ubiquitin Protein Ligase E3A
USER – Uracil-Specific Excision Reagent
USP47 – Ubiquitin Specific Peptidase 47
USP8 – Ubiquitin Specific Peptidase 8

Ethics approval

All *in vivo* experimental procedures were approved by La Trobe University (Ethics approval number: AEC21047) Animal Care and Use Committees and performed according to the guidelines set forth by the Australian Code for the Care and Use of Animals for Scientific Purposes (8th edition) and confirmed NIH Guide for the Care and Use of Laboratory Animals.

Acknowledgments

This work was supported by La Trobe University (start-up grant to Thiruma V. Arumugam), the National Health and Medical Research Council of Australia (Grant Identification Number 2019100), Institute of Molecular and Cell Biology, Agency for Science, Technology and Research, Singapore. S.D. is funded by the SINGA (Singapore International Graduate Award) fellowship. Figure 1 in this article was created using BioRender.

Author contributions

Study conception and design: T.V.A., Y.F., X.P., J.G., M.P.M., and D.G.J.; experiment or data collection: Y.F., X.P., N.I.T., X.C., V.L., and T.V.A.: data analysis: Y.F., S.D.S., X.P., and T.V.A.; data analytics and interpretation: Y.F., X.P., S.D.S., Y.K., and T.V.A.; writing-manuscript preparation and intellectual input: Y.F., S.D.S., X.P., Y.K., Y.U.L., G.C., E.O., T.G.J., C.G.S., J.G., M.K.P.L., M.P.M., D.G.J., and T.V.A.; supervision and administration: T.V.A.

Data availability

The mass spectrometry proteomics data will be deposited to the ProteomeXchange Consortium via the PRIDE partner repository. High throughput RNA sequencing data from this manuscript have been submitted to the NCBI Sequence Read Archive (SRA) under accession number GSE290224.

Competing interests

T.G.J. is affiliated with Epigenes Pty Ltd. The remaining authors declare no competing interests.

Figure 1

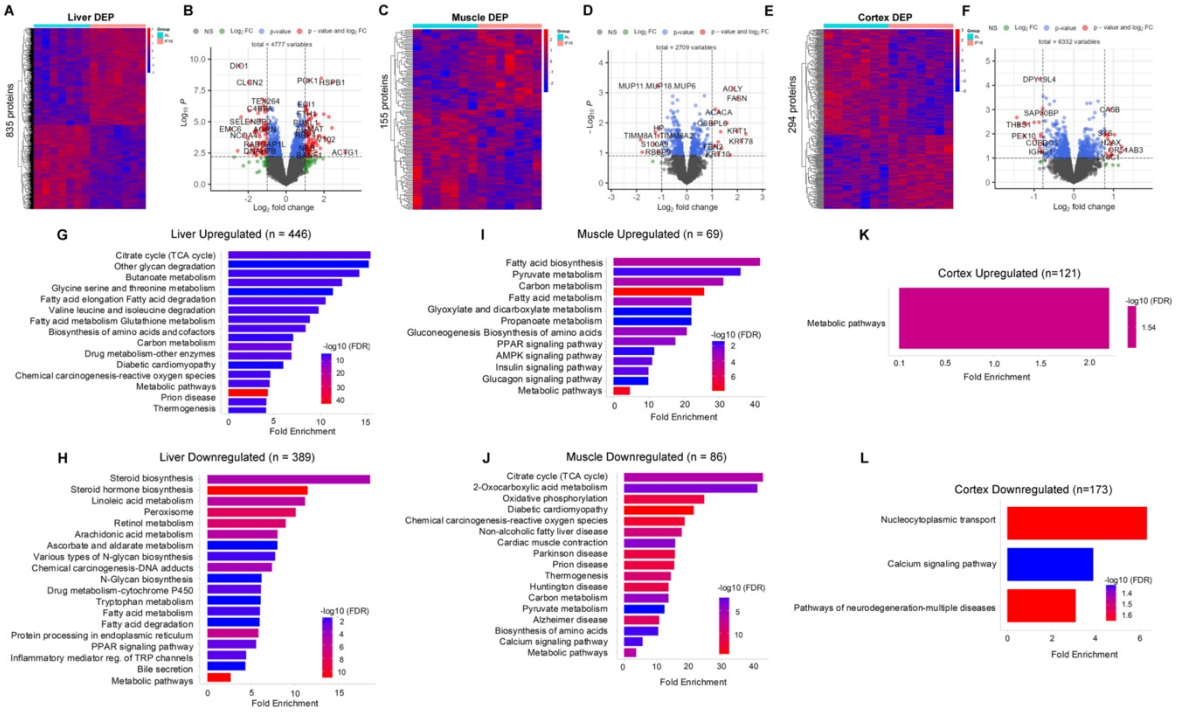

Figure 2

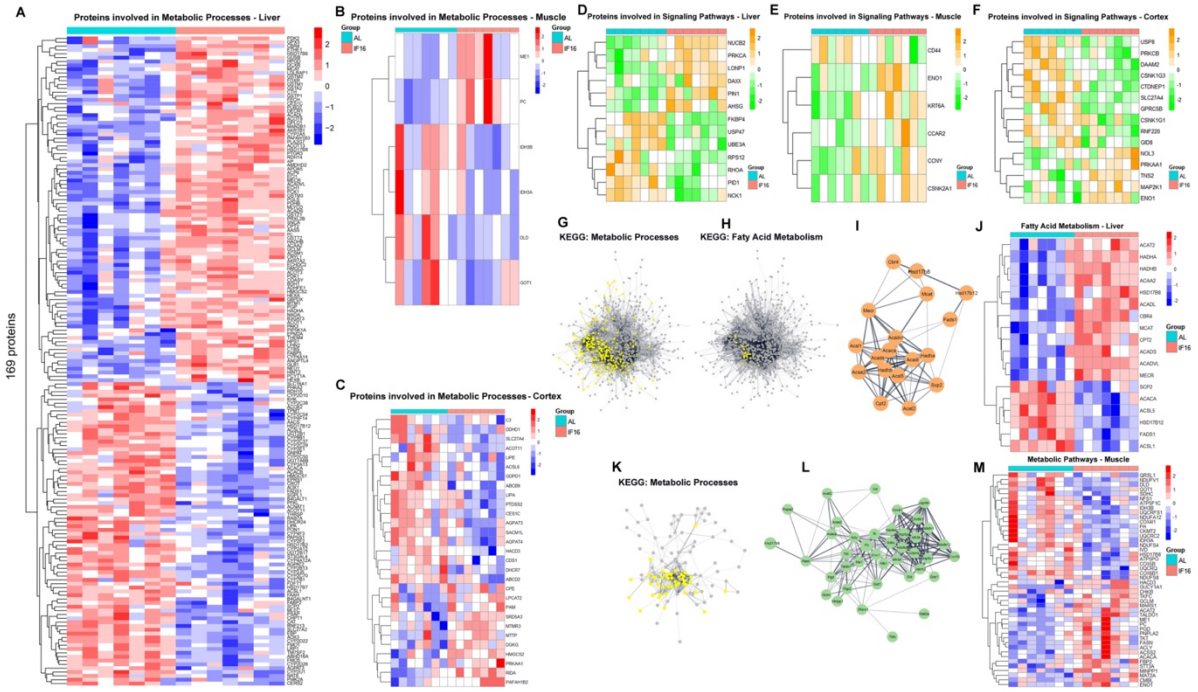

Figure 3

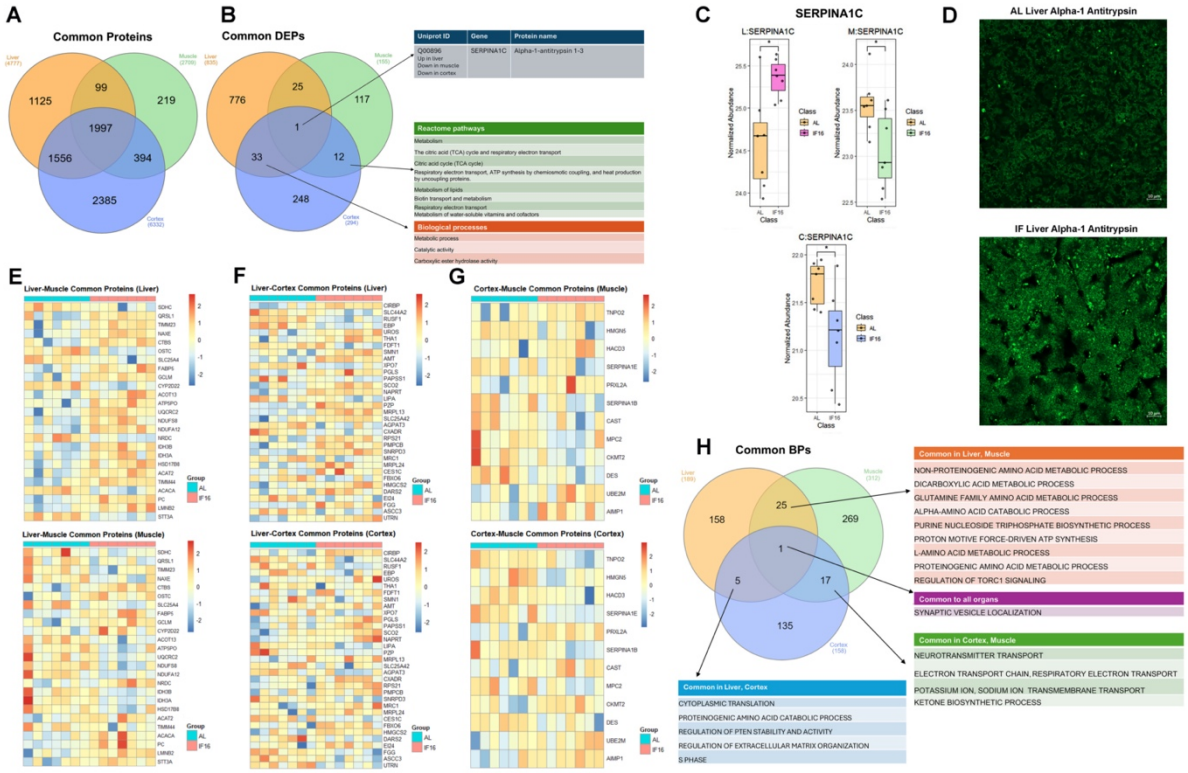
A
Common Proteins
Liver (4777)
Muscle (2709)
Cortex (6332)
1125
99
219
1997
1556
394
2385
B
Common DEPs
Liver (835)
Muscle (155)
Cortex (284)
776
25
117
1
33
12
248
Uniprot ID
Gene
Protein name
Q00896
SERPINA1C
Alpha-1-antitrypsin 1-3
Up in liver
Down in muscle
Down in cortex
Reactome pathways
Metabolism
The citric acid (TCA) cycle and respiratory electron transport
Citric acid cycle (TCA cycle)
Respiratory electron transport, ATP synthesis by chemiosmotic coupling, and heat production by uncoupling proteins.
Metabolism of lipids
Biotin transport and metabolism
Respiratory electron transport
Metabolism of water-soluble vitamins and cofactors
Biological processes
Metabolic process
Catalytic activity
Carboxylic ester hydrolase activity
C
SERPINA1C
L:SERPINA1C
M:SERPINA1C
C:SERPINA1C
Normalized Abundance
Class
AL
IF16
D
AL Liver Alpha-1 Antitrypsin
IF Liver Alpha-1 Antitrypsin
E
Liver-Muscle Common Proteins (Liver)
Liver-Muscle Common Proteins (Muscle)
F
Liver-Cortex Common Proteins (Liver)
Liver-Cortex Common Proteins (Cortex)
G
Cortex-Muscle Common Proteins (Muscle)
Cortex-Muscle Common Proteins (Cortex)
Group
H
Common BPs
Liver (169)
Muscle (312)
Cortex (158)
158
25
269
1
5
17
135
Common in Liver, Muscle
NON-PROTEINOGENIC AMINO ACID METABOLIC PROCESS
DICARBOXYLIC ACID METABOLIC PROCESS
GLUTAMINE FAMILY AMINO ACID METABOLIC PROCESS
ALPHA-AMINO ACID CATABOLIC PROCESS
PURINE NUCLEOSIDE TRIPHOSPHATE BIOSYNTHETIC PROCESS
PROTON MOTIVE FORCE-DRIVEN ATP SYNTHESIS
L-AMINO ACID METABOLIC PROCESS
PROTEINOGENIC AMINO ACID METABOLIC PROCESS
REGULATION OF TORC1 SIGNALING
Common to all organs
SYNAPTIC VESICLE LOCALIZATION
Common in Cortex, Muscle
NEUROTRANSMITTER TRANSPORT
ELECTRON TRANSPORT CHAIN, RESPIRATORY ELECTRON TRANSPORT
POTASSIUM ION, SODIUM ION TRANSMEMBRANE TRANSPORT
KETONE BIOSYNTHETIC PROCESS
Common in Liver, Cortex
CYTOPLASMIC TRANSLATION
PROTEINOGENIC AMINO ACID CATABOLIC PROCESS
REGULATION OF PTEN STABILITY AND ACTIVITY
REGULATION OF EXTRACELLULAR MATRIX ORGANIZATION
S PHASE

Figure 4

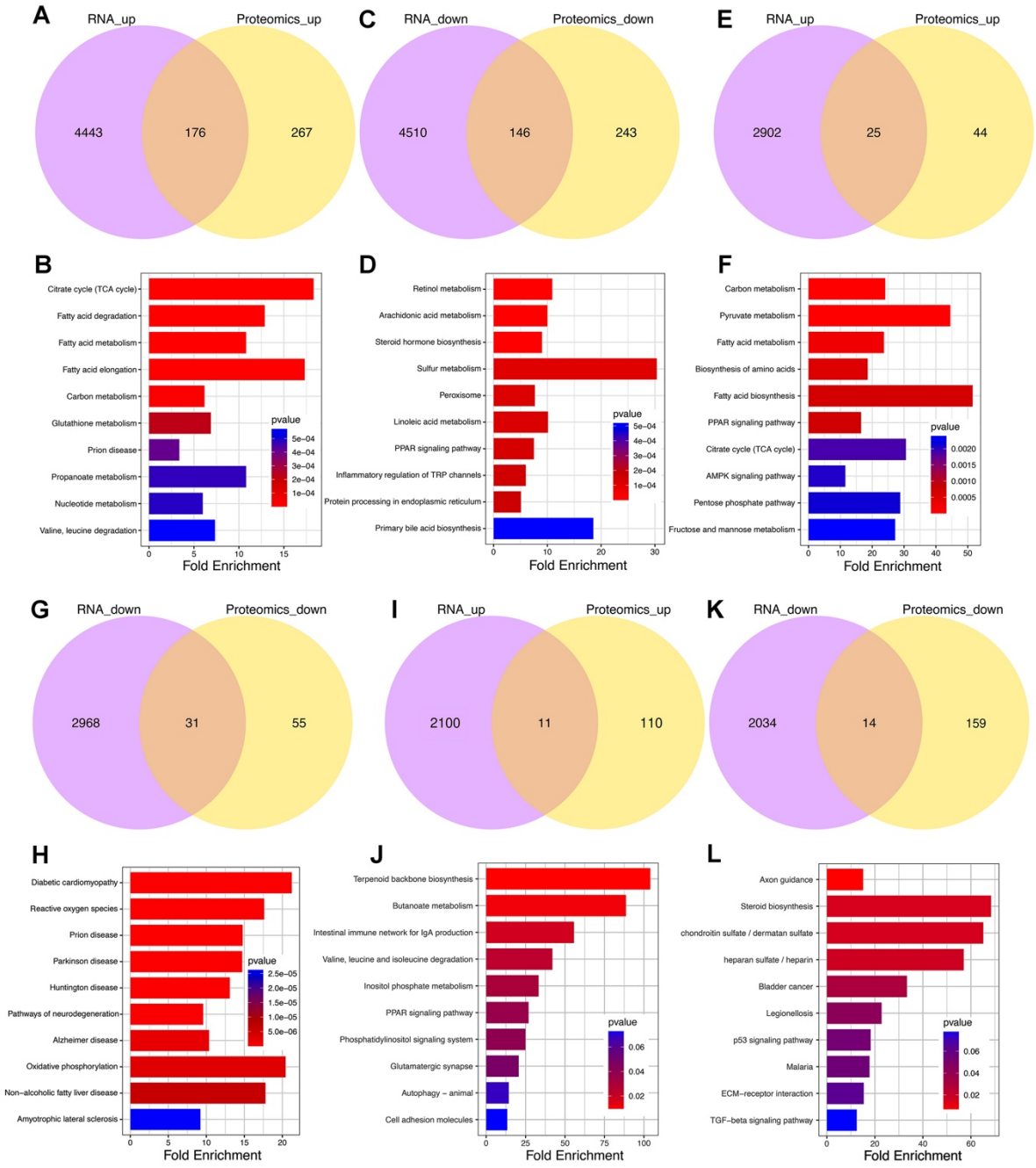
A
RNA_up
Proteomics_up
4443
176
267
C
RNA_down
Proteomics_down
4510
146
243
E
RNA_up
Proteomics_up
2902
25
44
B
Citrate cycle (TCA cycle)
Fatty acid degradation
Fatty acid metabolism
Fatty acid elongation
Carbon metabolism
Glutathione metabolism
Prion disease
Propanoate metabolism
Nucleotide metabolism
Valine, leucine degradation
pvalue
5e−04
4e−04
3e−04
2e−04
1e−04
Fold Enrichment
D
Retinol metabolism
Arachidonic acid metabolism
Steroid hormone biosynthesis
Sulfur metabolism
Peroxisome
Linoleic acid metabolism
PPAR signaling pathway
Inflammatory regulation of TRP channels
Protein processing in endoplasmic reticulum
Primary bile acid biosynthesis
pvalue
5e−04
4e−04
3e−04
2e−04
1e−04
Fold Enrichment
F
Carbon metabolism
Pyruvate metabolism
Fatty acid metabolism
Biosynthesis of amino acids
Fatty acid biosynthesis
PPAR signaling pathway
Citrate cycle (TCA cycle)
AMPK signaling pathway
Pentose phosphate pathway
Fructose and mannose metabolism
pvalue
0.0020
0.0015
0.0010
0.0005
Fold Enrichment
G
RNA_down
Proteomics_down
2968
31
55
I
RNA_up
Proteomics_up
2100
11
110
K
RNA_down
Proteomics_down
2034
14
159
H
Diabetic cardiomyopathy
Reactive oxygen species
Prion disease
Parkinson disease
Huntington disease
Pathways of neurodegeneration
Alzheimer disease
Oxidative phosphorylation
Non−alcoholic fatty liver disease
Amyotrophic lateral sclerosis
pvalue
2.5e−05
2.0e−05
1.5e−05
1.0e−05
5.0e−06
Fold Enrichment
J
Terpenoid backbone biosynthesis
Butanoate metabolism
Intestinal immune network for IgA production
Valine, leucine and isoleucine degradation
Inositol phosphate metabolism
PPAR signaling pathway
Phosphatidylinositol signaling system
Glutamatergic synapse
Autophagy − animal
Cell adhesion molecules
pvalue
0.06
0.04
0.02
Fold Enrichment
L
Axon guidance
Steroid biosynthesis
chondroitin sulfate / dermatan sulfate
heparan sulfate / heparin
Bladder cancer
Legionellosis
p53 signaling pathway
Malaria
ECM−receptor interaction
TGF−beta signaling pathway
pvalue
0.06
0.04
0.02
Fold Enrichment

S. Figure 1

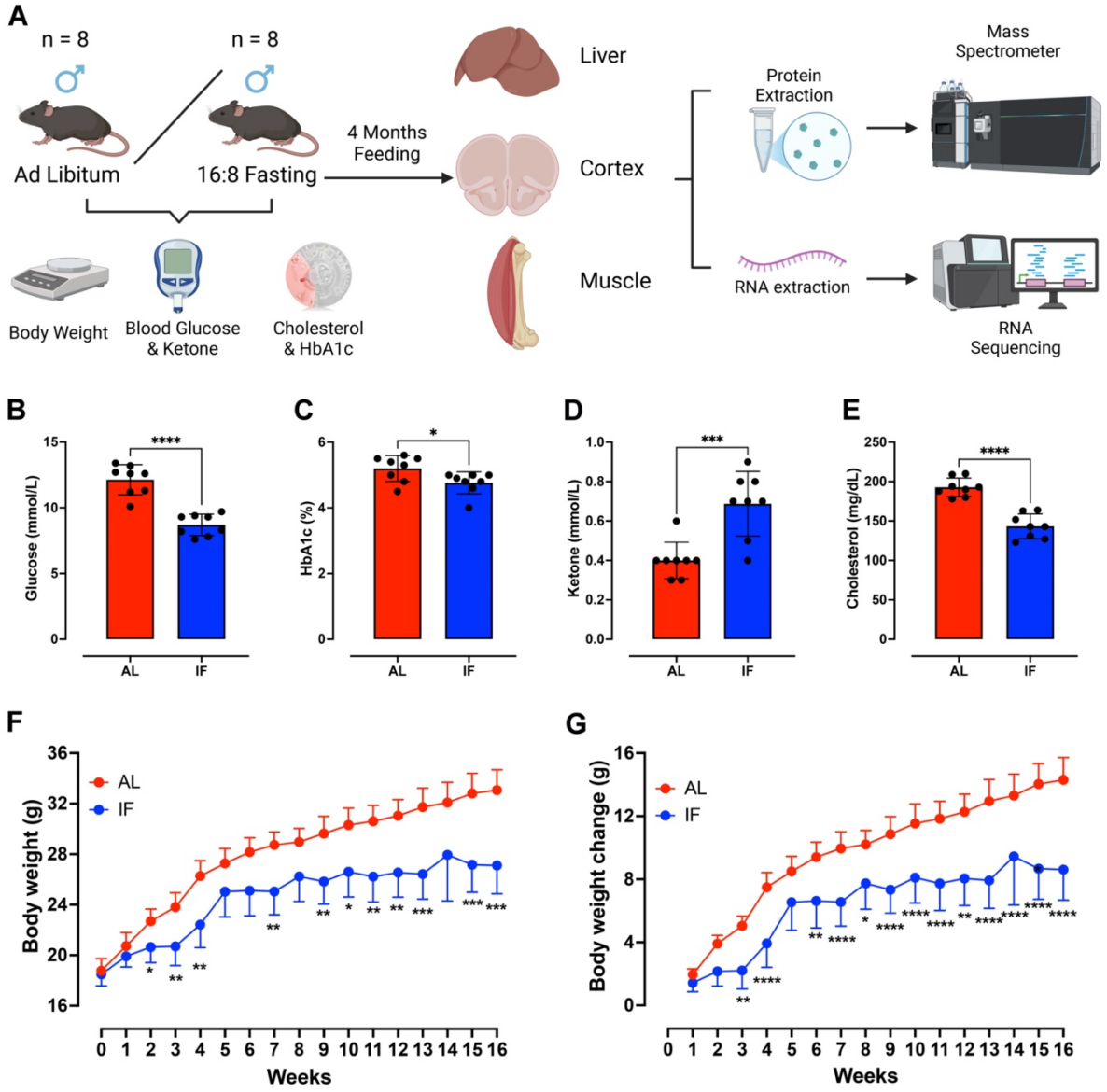
A
n = 8
n = 8
Ad Libitum
16:8 Fasting
4 Months Feeding
Liver
Cortex
Muscle
Protein Extraction
Mass Spectrometer
RNA extraction
RNA Sequencing
Body Weight
Blood Glucose & Ketone
Cholesterol & HbA1c
B
Glucose (mmol/L)
C
HbA1c (%)
D
Ketone (mmol/L)
E
Cholesterol (mg/dL)
AL
IF
F
Body weight (g)
G
Body weight change (g)
Weeks

S. Figure 2

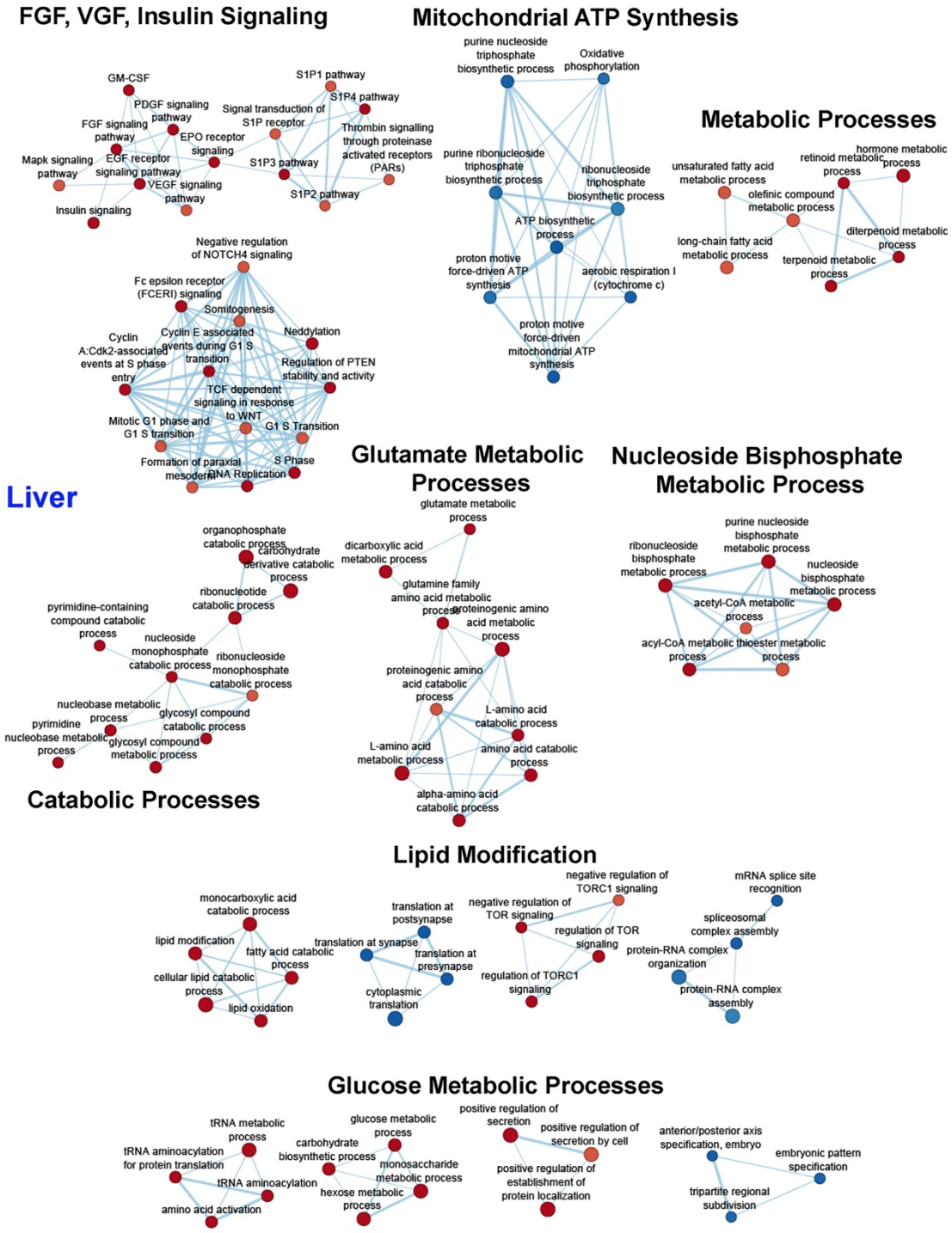
FGF, VGF, Insulin Signaling
GM-CSF
PDGF signaling pathway
FGF signaling pathway
EPO receptor signaling
Mapk signaling pathway
EGF receptor signaling pathway
VEGF signaling pathway
Insulin signaling
S1P1 pathway
S1P4 pathway
Signal transduction of S1P receptor
Thrombin signalling through proteinase activated receptors (PARs)
S1P3 pathway
S1P2 pathway
Mitochondrial ATP Synthesis
purine nucleoside triphosphate biosynthetic process
Oxidative phosphorylation
purine ribonucleoside triphosphate biosynthetic process
ribonucleoside triphosphate biosynthetic process
ATP biosynthetic process
proton motive force-driven ATP synthesis
aerobic respiration I (cytochrome c)
proton motive force-driven mitochondrial ATP synthesis
Metabolic Processes
unsaturated fatty acid metabolic process
retinoid metabolic process
hormone metabolic process
olefinic compound metabolic process
long-chain fatty acid metabolic process
diterpenoid metabolic process
terpenoid metabolic process
Negative regulation of NOTCH4 signaling
Fc epsilon receptor (FCERI) signaling
Somitogenesis
Cyclin A:Cdk2-associated events at S phase entry
Cyclin E associated events during G1 S transition
Neddylation
Regulation of PTEN stability and activity
TCF dependent signaling in response to WNT
Mitotic G1 phase and G1 S transition
G1 S Transition
Formation of paraxial mesoderm
S Phase
RNA Replication
Liver
Glutamate Metabolic Processes
glutamate metabolic process
dicarboxylic acid metabolic process
glutamine family amino acid metabolic process
proteinogenic amino acid metabolic process
proteinogenic amino acid catabolic process
L-amino acid catabolic process
L-amino acid metabolic process
amino acid catabolic process
alpha-amino acid catabolic process
Nucleoside Bisphosphate Metabolic Process
purine nucleoside bisphosphate metabolic process
ribonucleoside bisphosphate metabolic process
nucleoside bisphosphate metabolic process
acetyl-CoA metabolic process
acyl-CoA metabolic process
thioester metabolic process
organophosphate catabolic process
carbohydrate derivative catabolic process
ribonucleotide catabolic process
pyrimidine-containing compound catabolic process
nucleoside monophosphate catabolic process
ribonucleoside monophosphate catabolic process
nucleobase metabolic process
pyrimidine nucleobase metabolic process
glycosyl compound catabolic process
glycosyl compound metabolic process
Catabolic Processes
Lipid Modification
monocarboxylic acid catabolic process
lipid modification
fatty acid catabolic process
cellular lipid catabolic process
lipid oxidation
translation at postsynapse
translation at synapse
translation at presynapse
cytoplasmic translation
negative regulation of TORC1 signaling
negative regulation of TOR signaling
regulation of TOR signaling
regulation of TORC1 signaling
mRNA splice site recognition
spliceosomal complex assembly
protein-RNA complex organization
protein-RNA complex assembly
Glucose Metabolic Processes
tRNA metabolic process
tRNA aminoacylation for protein translation
tRNA aminoacylation
amino acid activation
glucose metabolic process
carbohydrate biosynthetic process
monosaccharide metabolic process
hexose metabolic process
positive regulation of secretion
positive regulation of secretion by cell
positive regulation of establishment of protein localization
anterior/posterior axis specification, embryo
embryonic pattern specification
tripartite regional subdivision

S. Figure 3

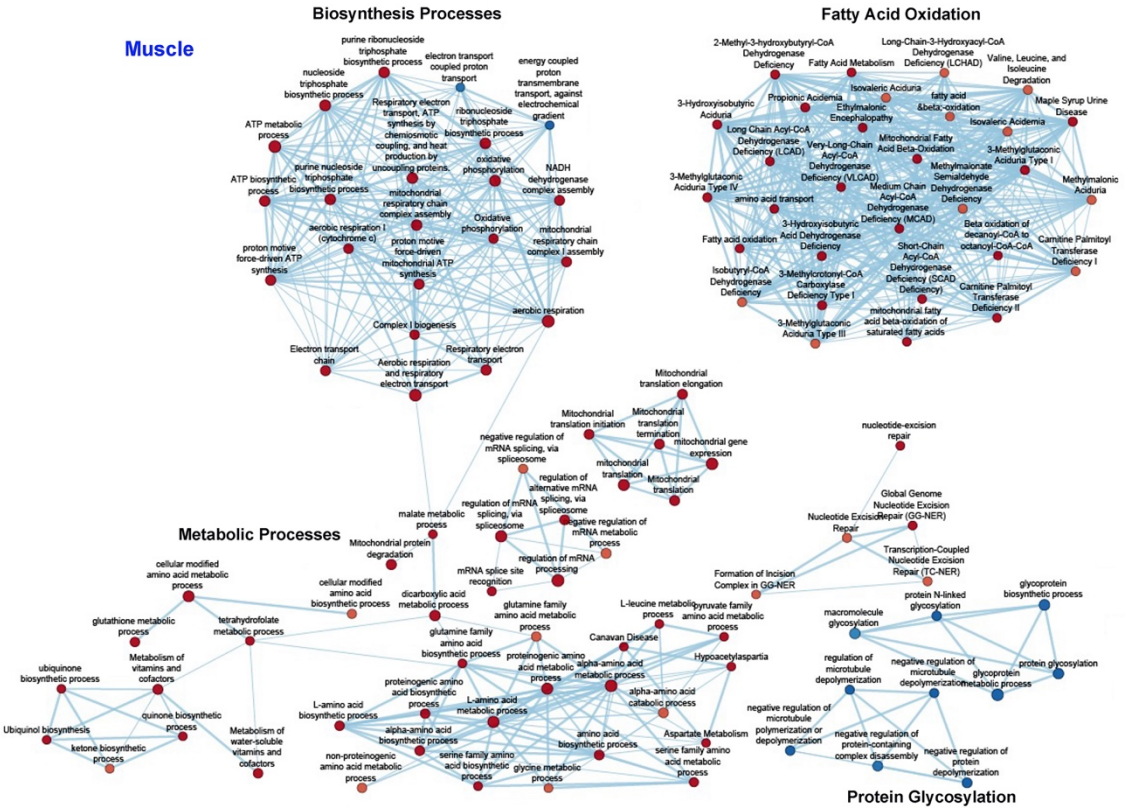
Muscle
Biosynthesis Processes
purine ribonucleoside triphosphate biosynthetic process
electron transport coupled proton transport
energy coupled proton transmembrane transport, against electrochemical gradient
nucleoside triphosphate biosynthetic process
Respiratory electron transport, ATP synthesis by chemiosmotic coupling, and heat production by uncoupling proteins.
ribonucleoside triphosphate biosynthetic process
ATP metabolic process
oxidative phosphorylation
NADH dehydrogenase complex assembly
purine nucleoside triphosphate biosynthetic process
ATP biosynthetic process
mitochondrial respiratory chain complex assembly
Oxidative phosphorylation
aerobic respiration I (cytochrome c)
mitochondrial respiratory chain complex I assembly
proton motive force-driven ATP synthesis
proton motive force-driven mitochondrial ATP synthesis
aerobic respiration
Complex I biogenesis
Electron transport chain
Respiratory electron transport
Aerobic respiration and respiratory electron transport
Fatty Acid Oxidation
2-Methyl-3-hydroxybutyryl-CoA Dehydrogenase Deficiency
Fatty Acid Metabolism
Long-Chain-3-Hydroxyacyl-CoA Dehydrogenase Deficiency (LCHAD)
Valine, Leucine, and Isoleucine Degradation
Isovaleric Aciduria
Propionic Acidemia
fatty acid β-oxidation
3-Hydroxyisobutyric Aciduria
Ethylmalonic Encephalopathy
Maple Syrup Urine Disease
Isovaleric Acidemia
Long Chain Acyl-CoA Dehydrogenase Deficiency (LCAD)
Very-Long-Chain Acyl-CoA Dehydrogenase Deficiency (VLCAD)
Mitochondrial Fatty Acid Beta-Oxidation
3-Methylglutaconic Aciduria Type I
Methylmalonate Semialdehyde Dehydrogenase Deficiency
3-Methylglutaconic Aciduria Type IV
Medium Chain Acyl-CoA Dehydrogenase Deficiency (MCAD)
Methylmalonic Aciduria
amino acid transport
3-Hydroxyisobutyric Acid Dehydrogenase Deficiency
Beta oxidation of decanoyl-CoA to octanoyl-CoA-CoA
Fatty acid oxidation
Short-Chain Acyl-CoA Dehydrogenase Deficiency (SCAD Deficiency)
Carnitine Palmitoyl Transferase Deficiency I
Isobutyryl-CoA Dehydrogenase Deficiency
3-Methylcrotonyl-CoA Carboxylase Deficiency Type I
Carnitine Palmitoyl Transferase Deficiency II
mitochondrial fatty acid beta-oxidation of saturated fatty acids
3-Methylglutaconic Aciduria Type III
Mitochondrial translation elongation
Mitochondrial translation initiation
Mitochondrial translation termination
mitochondrial gene expression
negative regulation of mRNA splicing, via spliceosome
mitochondrial translation
Mitochondrial translation
regulation of alternative mRNA splicing, via spliceosome
regulation of mRNA splicing, via spliceosome
negative regulation of mRNA metabolic process
nucleotide-excision repair
Global Genome Nucleotide Excision Repair (GG-NER)
Nucleotide Excision Repair
Transcription-Coupled Nucleotide Excision Repair (TC-NER)
Formation of Incision Complex in GG-NER
Metabolic Processes
malate metabolic process
Mitochondrial protein degradation
regulation of mRNA processing
mRNA splice site recognition
cellular modified amino acid metabolic process
cellular modified amino acid biosynthetic process
dicarboxylic acid metabolic process
glutamine family amino acid metabolic process
L-leucine metabolic process
pyruvate family amino acid metabolic process
glycoprotein biosynthetic process
protein N-linked glycosylation
macromolecule glycosylation
glutathione metabolic process
tetrahydrofolate metabolic process
glutamine family amino acid biosynthetic process
Canavan Disease
Hypoacetylaspartia
Metabolism of vitamins and cofactors
ubiquinone biosynthetic process
proteinogenic amino acid metabolic process
alpha-amino acid metabolic process
proteinogenic amino acid biosynthetic process
alpha-amino acid catabolic process
regulation of microtubule depolymerization
negative regulation of microtubule depolymerization
protein glycosylation
glycoprotein metabolic process
L-amino acid biosynthetic process
L-amino acid metabolic process
negative regulation of microtubule polymerization or depolymerization
quinone biosynthetic process
Ubiquinol biosynthesis
alpha-amino acid biosynthetic process
amino acid biosynthetic process
Aspartate Metabolism
negative regulation of protein-containing complex disassembly
Metabolism of water-soluble vitamins and cofactors
ketone biosynthetic process
non-proteinogenic amino acid metabolic process
serine family amino acid biosynthetic process
glycine metabolic process
serine family amino acid metabolic process
negative regulation of protein depolymerization
Protein Glycosylation

S. Figure 4

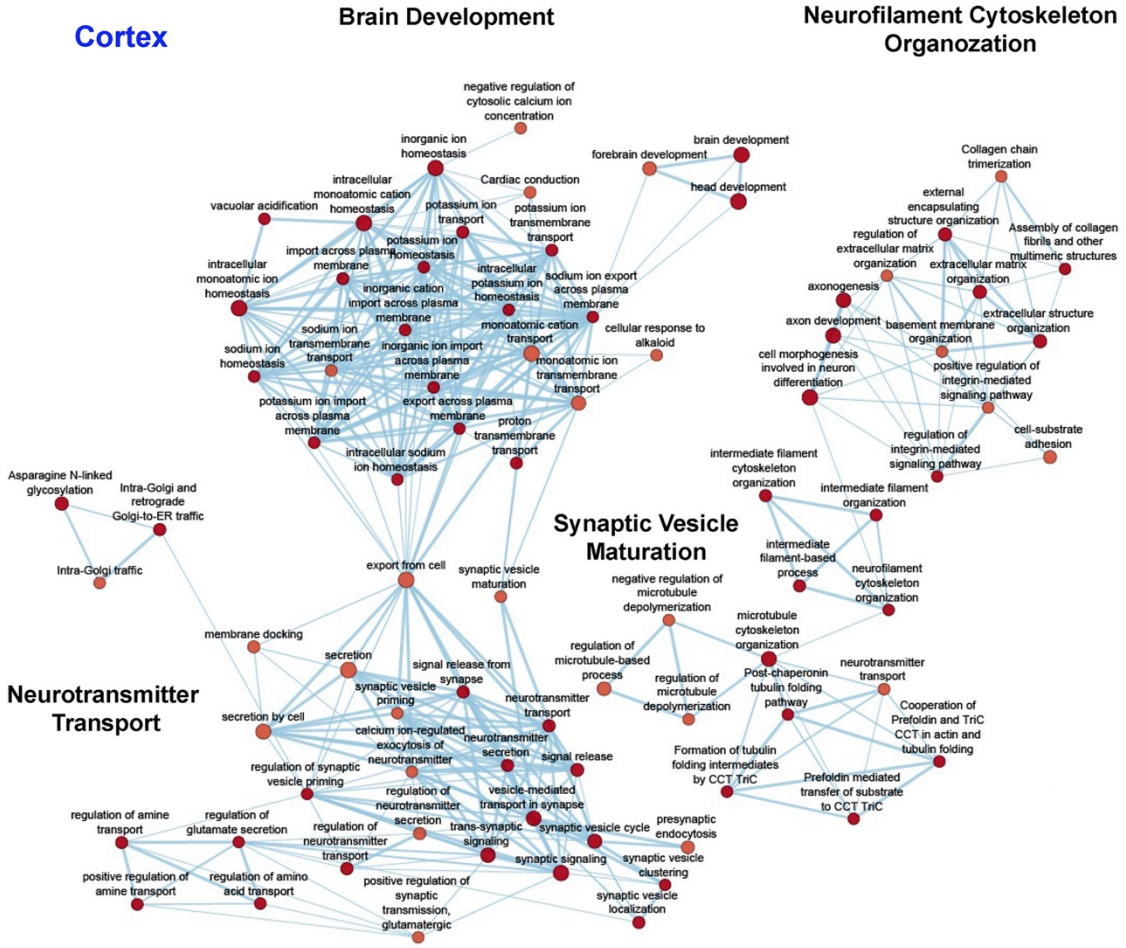
Cortex
Brain Development
Neurofilament Cytoskeleton Organozation
Synaptic Vesicle Maturation
Neurotransmitter Transport
negative regulation of cytosolic calcium ion concentration
inorganic ion homeostasis
brain development
forebrain development
head development
Collagen chain trimerization
intracellular monoatomic cation homeostasis
Cardiac conduction
vacuolar acidification
potassium ion transport
potassium ion transmembrane transport
external encapsulating structure organization
Assembly of collagen fibrils and other multimeric structures
regulation of extracellular matrix organization
extracellular matrix organization
import across plasma membrane
potassium ion homeostasis
intracellular monoatomic ion homeostasis
intracellular potassium ion homeostasis
sodium ion export across plasma membrane
axonogenesis
inorganic cation import across plasma membrane
extracellular structure organization
axon development
basement membrane organization
sodium ion transmembrane transport
monoatomic cation transport
cellular response to alkaloid
sodium ion homeostasis
inorganic ion import across plasma membrane
cell morphogenesis involved in neuron differentiation
positive regulation of integrin-mediated signaling pathway
monoatomic ion transmembrane transport
potassium ion import across plasma membrane
export across plasma membrane
proton transmembrane transport
cell-substrate adhesion
regulation of integrin-mediated signaling pathway
intermediate filament cytoskeleton organization
intracellular sodium ion homeostasis
Asparagine N-linked glycosylation
Intra-Golgi and retrograde Golgi-to-ER traffic
intermediate filament organization
Intra-Golgi traffic
export from cell
synaptic vesicle maturation
intermediate filament-based process
neurofilament cytoskeleton organization
negative regulation of microtubule depolymerization
microtubule cytoskeleton organization
membrane docking
secretion
signal release from synapse
regulation of microtubule-based process
regulation of microtubule depolymerization
Post-chaperonin tubulin folding pathway
neurotransmitter transport
synaptic vesicle priming
neurotransmitter transport
Cooperation of Prefoldin and TriC CCT in actin and tubulin folding
secretion by cell
calcium ion-regulated exocytosis of neurotransmitter
neurotransmitter secretion
signal release
Formation of tubulin folding intermediates by CCT TriC
regulation of synaptic vesicle priming
regulation of neurotransmitter secretion
vesicle-mediated transport in synapse
Prefoldin mediated transfer of substrate to CCT TriC
regulation of amine transport
regulation of glutamate secretion
regulation of neurotransmitter transport
trans-synaptic signaling
synaptic vesicle cycle
presynaptic endocytosis
synaptic signaling
synaptic vesicle clustering
positive regulation of amine transport
regulation of amino acid transport
positive regulation of synaptic transmission, glutamatergic
synaptic vesicle localization

S. Figure 5

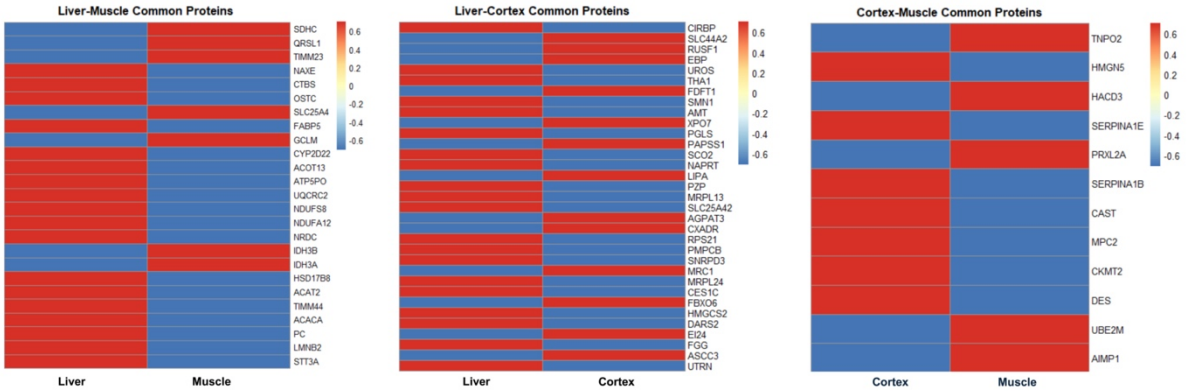

S. Figure 6

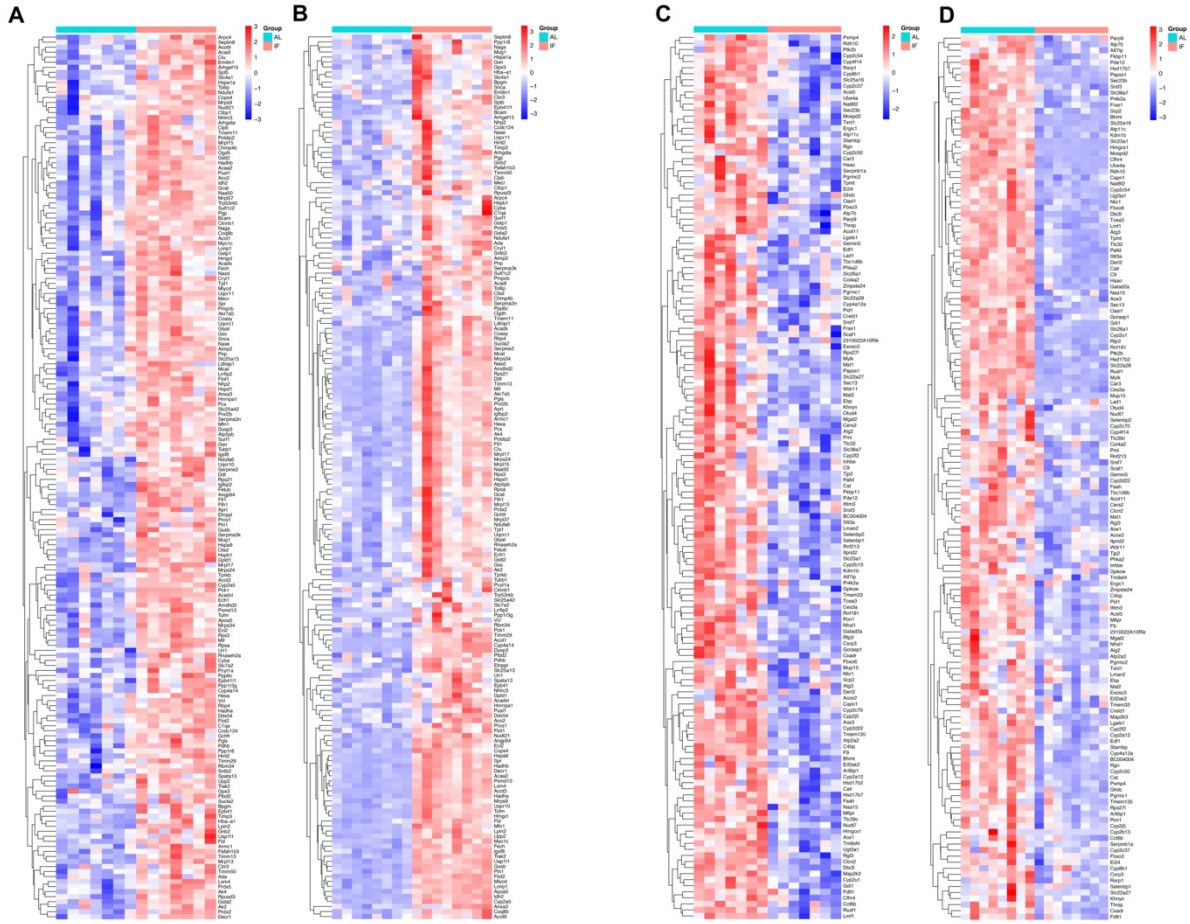

S. Figure 7

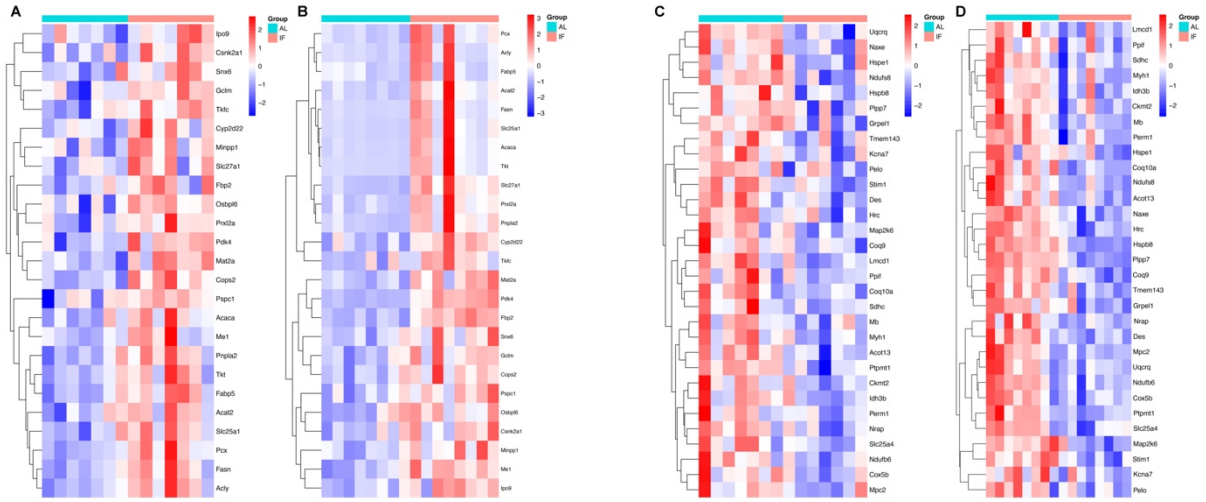
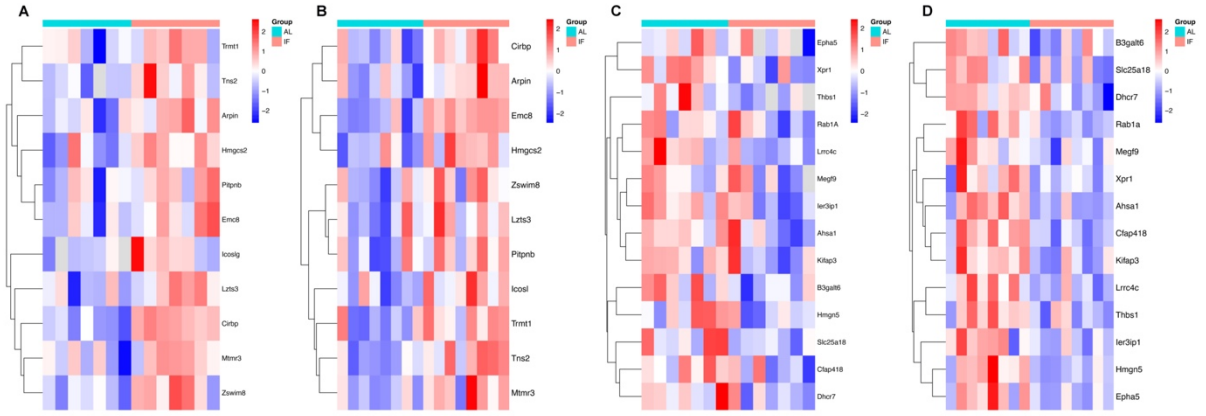
S. Figure 8